Article

Zika virus elicits inflammation to evade antiviral response by cleaving cGAS via NS1-caspase-1 axis

Yanyan Zheng[1,†], Qingxiang Liu[1,†], Yaoxing Wu[1,†] [iD], Ling Ma[2], Zhenzhen Zhang[2], Tao Liu[1], Shouheng Jin[1], Yuanchu She[1], Yi-Ping Li[2,3,*] [iD] & Jun Cui[1,**] [iD]

Abstract

Viral infection triggers host innate immune responses, which primarily include the activation of type I interferon (IFN) signaling and inflammasomes. Here, we report that Zika virus (ZIKV) infection triggers NLRP3 inflammasome activation, which is further enhanced by viral non-structural protein NS1 to benefit its replication. NS1 recruits the host deubiquitinase USP8 to cleave K11-linked polyubiquitin chains from caspase-1 at Lys134, thus inhibiting the proteasomal degradation of caspase-1. The enhanced stabilization of caspase-1 by NS1 promotes the cleavage of cGAS, which recognizes mitochondrial DNA release and initiates type I IFN signaling during ZIKV infection. NLRP3 deficiency increases type I IFN production and strengthens host resistance to ZIKV in vitro and in vivo. Taken together, our work unravels a novel antagonistic mechanism employed by ZIKV to suppress host immune response by manipulating the interplay between inflammasome and type I IFN signaling, which might guide the rational design of therapeutics in the future.

Introduction

Zika virus (ZIKV) is an arthropod-borne flavivirus in the *Flaviviridae* family, which was initially discovered from Rhesus macaque in Uganda in 1947 (Dick *et al*, 1952). ZIKV contains a positive-sense single-stranded RNA genome and is closely related to several other important viruses that cause disease globally, including Dengue (DENV), hepatitis C, yellow fever, West Nile, and Japanese encephalitis viruses (Pierson & Diamond, 2013). ZIKV genome encodes a single polyprotein which can be processed to produce three structural (C,

prM, and E) and seven non-structural (NS1, NS2A, NS2B, NS3, NS4A, NS4B, and NS5) proteins (Pierson & Diamond, 2013). ZIKV infection was originally thought as a mild and self-limiting viral illness and caught little attention (Rossi *et al*, 2016; Miner & Diamond, 2017). However, it became a global health emergency since accumulating evidence has suggested that ZIKV infection is associated with the increasing incidence of microcephaly in newborns and Guillain–Barré syndrome during the outbreak of ZIKV in Brazil from 2015 (Ioos *et al*, 2014; Petersen *et al*, 2016; Rubin *et al*, 2016).

Type I interferon (IFN) response serves as the first line of defense to combat viral infection (Schneider *et al*, 2014). Recently, we and other groups have demonstrated that ZIKV evolved several strategies to counter human IFN antiviral response (Fernandez-Garcia *et al*, 2009; Grant *et al*, 2016; Kumar *et al*, 2016; Wu *et al*, 2017; Xia *et al*, 2018). The IFN-antagonistic strategies can be mainly divided into two types (Fernandez-Garcia *et al*, 2009): The first strategy employed by ZIKV is to reduce and delay the activation of IFN production. For example, we recently reported that NS1 and NS4B of ZIKV blocked virus-mediated IFN signaling by targeting TBK1 (Wu *et al*, 2017). Xia *et al* showed the similar result of NS1 and found that residue 188 is critical for the inhibition of IFN (Xia *et al*, 2018). ZIKV could also utilize the other strategy to evade innate immunity by antagonizing IFN-mediated downstream signaling transduction. It has been reported that NS5 of ZIKV promoted the degradation of STAT2 (Grant *et al*, 2016; Kumar *et al*, 2016), while our study also revealed that NS2B3 can degrade JAK1 (Wu *et al*, 2017), thus inhibiting JAK-STAT signaling and coincidentally impairing downstream ISG expressions. Taken together, different non-structural proteins of ZIKV attenuate innate antiviral response at different levels of IFN signaling pathway and cooperatively assist ZIKV to evade host immune response (Bowen *et al*, 2018).

To infect the fetus and affect the neural development of fetus, ZIKV should first cross the placental barrier and reach the fetus (Li *et al*, 2016; Miner *et al*, 2016). However, there is no commonly accepted mechanism employed by ZIKV to achieve mother-to-fetus transmission so far. One of the possible mechanisms utilized by ZIKV is to use monocytes as the carrier (Parekh *et al*, 2010; Khaiboullina *et al*, 2017). Monocytes are able to detect several kinds of pathogens and

1   MOE Key Laboratory of Gene Function and Regulation, State Key Laboratory of Biocontrol, School of Life Sciences, Sun Yat-sen University, Guangzhou, Guangdong, China
2   Institute of Human Virology, Key Laboratory of Tropical Diseases Control Ministry of Education, Zhongshan School of Medicine, Sun Yat-sen University, Guangzhou, China
3   Department of Infectious Disease, The Fifth Affiliated Hospital of Sun Yat-sen University, Zhuhai, China
    *Corresponding author. Tel: +86 20 87335085; E-mail: lyiping@mail.sysu.edu.cn
    **Corresponding author. Tel: +86 20 39943429; E-mail: cuij5@mail.sysu.edu.cn
    †These authors contributed equally to this work

respond with the activation of inflammasome, a large signaling protein complex whose assembly usually requires the protein apoptosis-associated speck-like protein containing a CARD (ASC), caspases, and scaffold proteins (such as NLRP3 or AIM2) (Martinon *et al*, 2009). Once activated, the inflammasome triggers the activation of the cysteine protease caspase-1 to prompt the maturation and secretion of the pro-inflammatory cytokines interleukin-1β (IL-1β) and IL-18 (Park *et al*, 2007; Liu *et al*, 2016). IL-1β serves the central role in inflammatory response and initiates a series of innate immune responses (Dinarello, 2009). Recently, accumulating evidence has revealed that ZIKV can infect monocytes and result in the activation of inflammasome pathway (Khaiboullina *et al*, 2017; Tricarico *et al*, 2017; Wang *et al*, 2018). However, the correlation between inflammasome activation and ZIKV infection remains incompletely understood.

Here, we report that ZIKV activates host inflammasome responses by increasing the stabilization of caspase-1. Interestingly, ZIKV NS1 targets caspase-1 and removes its K11-linked ubiquitin chains at lysine (Lys) 134 by recruiting deubiquitinase (DUB) USP8. Consequently, caspase-1 targets to cGAS for cleavage, which results in reduced type I IFN signaling and enhanced ZIKV replication. Furthermore, NLRP3 deficiency increases type I IFN production and strengthens host resistance to ZIKV *in vivo*. Taken together, we identify a novel function of ZIKV NS1 in regulating the stability of caspase-1 and therefore reveal a mechanism by which ZIKV evades host antiviral response via initiating inflammasome activation. Our findings will facilitate the development of antiviral inhibitors and vaccine design toward novel strategies against ZIKV infection.

Results

ZIKV infection induces NLRP3 inflammasome activation

The inflammasome plays a key role in host innate immune responses by promoting pro-caspase-1 cleavage to generate the active subunits p20 and p10, leading to the maturation and secretion of IL-1β. In order to determine whether ZIKV infection activates the inflammasomes, we measured IL-1β secretion from unprimed or lipopolysaccharide (LPS)-primed THP-1 cells (a human monocyte cell line) infected with ZIKV (Asian lineage strain GZ01 (GenBank No. KU820898) if not specified). Immunoblot and ELISA analyses demonstrated that ZIKV infection induced the release of IL-1β from both unprimed and LPS-primed THP-1 cells (Fig 1A and B). NLRP3 and AIM2 are known to play important roles in inflammasome activation by virus infection (Martinon *et al*, 2009). We next generated NLRP3 and AIM2 knockout (KO) THP-1 cells by CRISPR/Cas9 technology (Fig EV1A), and KO efficiency was functionally validated by LPS plus ATP or poly (dA:dT) treatment as positive or negative controls. We found that ZIKV-induced IL-1β and IL-18 secretion as well as caspase-1 cleavage was abrogated in NLRP3 KO THP-1 cells but not in AIM2 KO THP-1 cells (Figs 1C and EV1B–D). To further confirm the induction of NLRP3 inflammasome by ZIKV, we examined IL-1β secretion in two different clones of NLRP3 or AIM2 KO cells at various time points after ZIKV infection and got consistent results (Figs 1D and EV1E). Moreover, we found that knockdown of *NLRP3* by two different siRNAs suppressed IL-1β secretion after ZIKV infection in human peripheral blood mononuclear cells (PBMCs) from two healthy donors (Figs 1E and EV1F). We also examined another ZIKV recombinant (MR766)—a historical African lineage strain (Dick *et al*, 1952; Schwarz *et al*, 2016), which differs from GZ01 by 11% at nucleotide level. We found that both African strain MR766 and Asian strain GZ01 induced NLRP3 inflammasome activation (Fig 1F). In addition, we compared ZIKV with Dengue virus serotype 2 (DENV-2) strain 16681 (Pu *et al*, 2011), a flavivirus closely related to ZIKV, and found that compared with ZIKV, DENV-2 only induced weak inflammasome activation (Fig 1F). Taken together, these results demonstrate that ZIKV infection specifically activates the NLRP3 inflammasome.

A number of viruses have evolved mechanisms to prolong their intracellular survival by inhibiting the inflammasome activation (Komune *et al*, 2011; Cheong *et al*, 2015). However, we observed that ZIKV infection promotes the activation of inflammasomes, since more cleaved IL-1β was detected in THP-1 cells infected with ZIKV followed by LPS and ATP treatment to activate NLRP3

Figure 1. The non-structural protein NS1 of ZIKV enhances ZIKV-induced NLRP3 inflammasome activation.

A   ELISA of supernatant IL-1β for unprimed THP-1 cells (UT) or LPS-primed (500 ng/ml, 3 h) THP-1 cells infected with ZIKV (MOI = 1) for 36 h. Uninfected cells serve as mock control.

B   Immunoblot analysis of supernatant (Sup) and cell extracts (Lys) of THP-1 cells, left untreated, or primed by LPS (500 ng/ml, 3 h), after ZIKV infection (MOI = 1) for 36 h.

C   ELISA of IL-1β in the supernatants of wild type (WT), NLRP3 knockout (KO) #1, or AIM2 KO#1 THP-1 cells left untreated (UT), or pre-treated with LPS (500 ng/ml, 3 h) followed by ATP (5 mM, 6 h) stimulation, or stimulated with poly (dA:dT) (1 mg/ml, 6 h), or infected with ZIKV (MOI = 1, 36 h).

D   ELISA of IL-1β in the supernatants of two clones of NLRP3 KO THP-1 cells with or without ZIKV infection (MOI = 1) at the indicated time points.

E   ELISA of IL-1β in the supernatants of PBMCs from two donors transfected with control (ctrl) siRNA or *NLRP3* siRNA followed by ZIKV infection (MOI = 1) for 36 h.

F   ELISA of IL-1β in the supernatant of WT, NLRP3 KO, or AIM2 KO THP-1 cells with ZIKV (MR766 or GZ01) (MOI = 1) or DENV-2 (MOI = 1) infection for 36 h.

G   ELISA of IL-1β in the supernatants of THP-1 cells pre-infected with ZIKV for 24 h or mock control. The cells were then treated with LPS (500 ng/ml, 3 h) followed by ATP (5 mM) treatment for 6 h.

H   Immunoblot analysis of supernatant (Sup) and cell extracts (Lys) of THP-1 cells pre-infected with ZIKV (MOI = 1) or mock control for 24 h. The cells were then treated with LPS (500 ng/ml, 3 h) followed by ATP (5 mM) stimulation for 6 h.

I   Immunoblot analysis of supernatants and cell extracts of 293T cells transfected with plasmids expressing NLRP3, ASC, pro-caspase-1, and pro-IL-1β together with NS1.

J   Immunoblot analysis of protein extracts of Flag-tagged NS1-inducible THP-1 cells treated with increasing doses of doxycycline (Dox) for 24 h.

K   ELISA of IL-1β in the supernatants of Flag-NS1-inducible THP-1 cells left unprimed then treated with ATP (5 mM, 6 h) or poly (I:C) (2 mg/ml, 6 h), or pre-treated with LPS (500 ng/ml, 3 h) followed by ATP (5 mM, 6 h) or poly (I:C) (2 mg/ml, 6 h) stimulation.

L   Immunoblot analysis of supernatants (Sup) and cell extracts (Lys) of Flag-NS1-inducible THP-1 cells pre-treated with LPS (500 ng/ml, 3 h) followed by ATP (5 mM, 6 h) or poly (I:C) (2 mg/ml, 6 h) stimulation.

Data information: In (B, H–J, L), data are representative of three independent experiments. In (A, C, D–G, K), data are mean values ± SEM (*n* = 3). NS (non-significant), *P* > 0.05; *P < 0.05; **P < 0.01; ***P < 0.001.
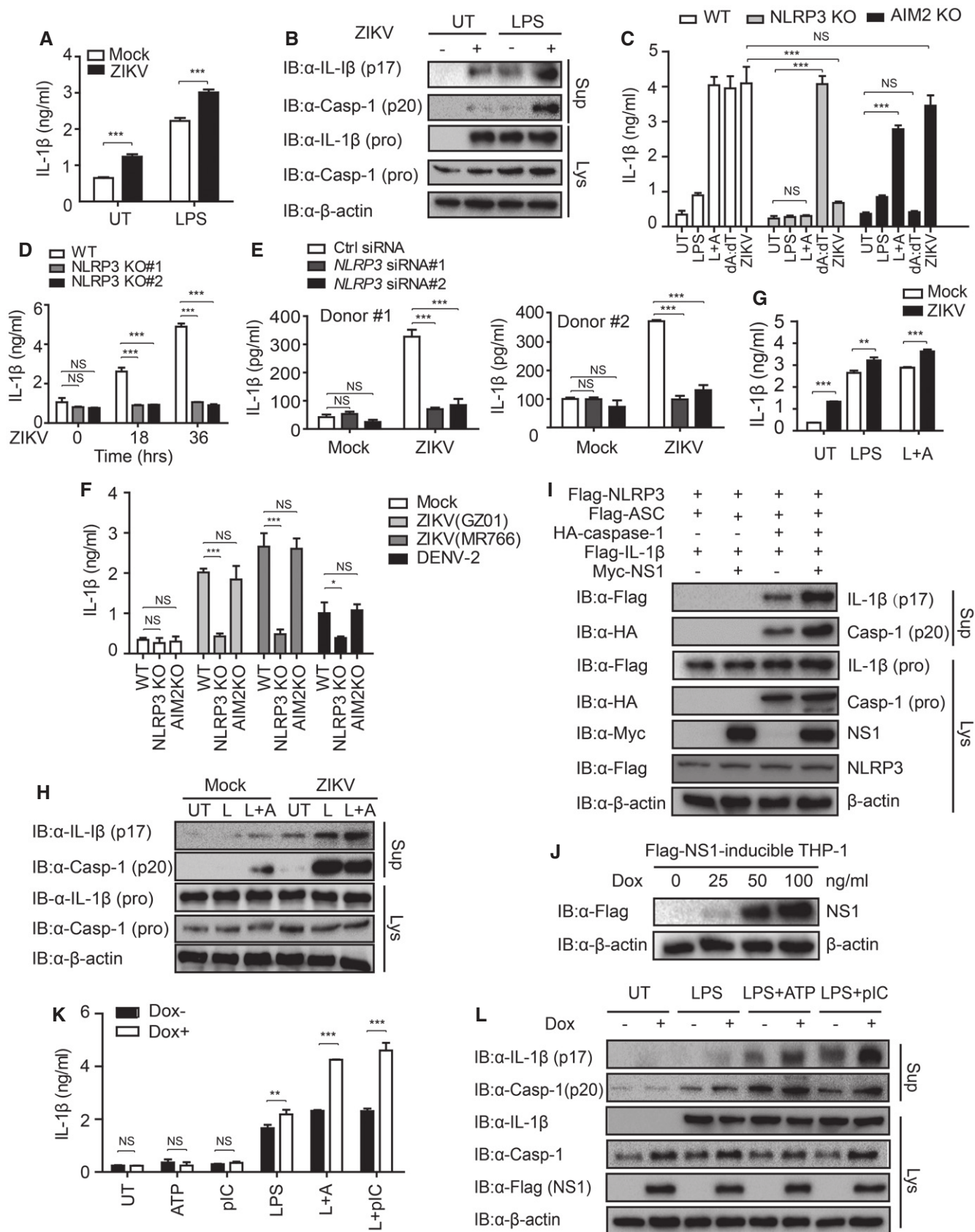
Source data are available online for this figure.

Figure 1.

inflammasome (Fig 1G and H). Meanwhile, ZIKV infection did not affect the inflammasome activation-induced cell death (Fig EV1G). Together, these results suggest that ZIKV infection triggers NLRP3 inflammasome activation.

The non-structural protein NS1 of ZIKV enhances inflammasome activation

Next, we set out to unveil the underlying mechanisms through which ZIKV promotes inflammasome activation. The non-structural protein 1 (NS1) is the major host-interaction molecule that functions in flavivirus replication, pathogenesis, and immune evasion (Hilgenfeld, 2016). To evaluate whether NS1 of ZIKV plays a role in inflammasome activation, we utilized human embryonic kidney (HEK) 293T cells in which the NLRP3 inflammasome is deficient and can be reconstituted. Overexpression of NS1 but not NS2B3 or NS4B of ZIKV led to a profound inflammasome activation, as characterized by the increased secretion of mature caspase-1 and IL-1β into the culture medium (Figs 1I and EV1H). To further confirm these results, we generated a doxycycline (Dox)-inducible NS1 THP-1 cell line (Fig 1J). After LPS priming and ATP or poly (I:C) stimulation, more mature IL-1β and cleaved caspase-1 could be detected when NS1 was induced to express (Figs 1K and L, and EV1I). Taken together, these results demonstrate that NS1 further facilitates NLRP3 inflammasome activation during ZIKV infection.

The enhanced inflammasome activation by NS1 benefits ZIKV infection

In light of the critical role of the inflammasome in the host antiviral responses, we turned our attention to its impact on ZIKV replication. Surprisingly, we observed a significantly higher accumulation of ZIKV viral RNA in LPS and ATP pre-treated THP-1 cells (Fig 2A). Consistently, knockout (KO) of NLRP3 in THP-1 cells resulted in lower viral replication (Fig 2B). To further confirm this finding, we examined ZIKV replication in bone marrow-derived macrophages (BMDMs) from NLRP3-deficient ($Nlrp3^{-/-}$) mice (Fig 2C) by qRT–PCR as well as plaque titration assay. The results showed that the level of ZIKV RNA (Fig 2D) and virus titer (Fig 2E) was significantly lower in $Nlrp3^{-/-}$ BMDMs, compared to that of wild-type (WT) BMDMs. We next generated caspase-1 KO THP-1 cells (Fig 2F) and found that caspase-1 deficiency also decreased ZIKV replication (Fig 2G). Moreover, the use of Ac-YVAD-cmk (YVAD for short), a specific inhibitor of caspase-1, attenuated ZIKV replication (Fig EV2A), indicating that the reinforcing effect of NLRP3 inflammasome on ZIKV replication relied on the enzyme activity of caspase-1. Consistently, NS1-induced up-regulation of ZIKV replication could be blocked by YVAD (Fig 2H), indicating that NS1 also functions through caspase-1 activity. To validate these findings in human primary cells, we knocked down *NLRP3* by siRNA in PBMCs from two different healthy donors (Fig 2I). We observed lower viral replication after knockdown of *NLRP3* (Fig 2J). Furthermore, YVAD treatment in PBMCs also suppressed ZIKV replication (Fig 2K). We next examined whether MR766 strain shared the same property as GZ01 strain and found that NLRP3 deficiency inhibited the viral replication of both strains (Fig EV2B). Since NLRP3 inflammasome activation is sufficient to drive pro-IL-1β processing and secretion, we therefore assessed the contribution of IL-1β to this course. However, we found

that the replication of ZIKV was not affected by IL-1β treatment (Fig EV2C). Taken together, these data suggest that the enhanced NLRP3 inflammasome activation by NS1 benefits to ZIKV replication, which is dependent on the activity of caspase-1 but not IL-1β.
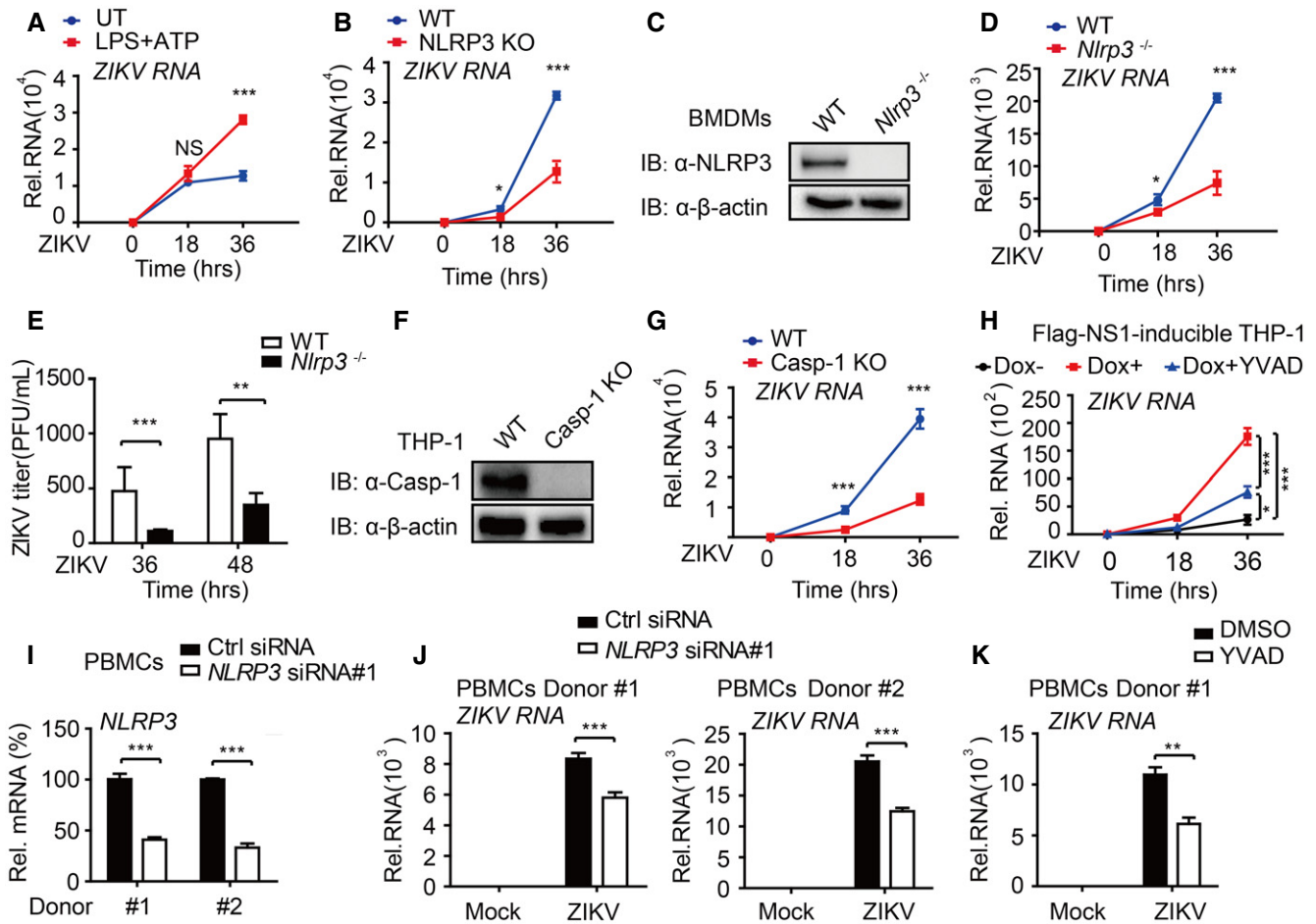
NS1 inhibits the proteasomal degradation of caspase-1

To dissect the molecular mechanisms by which NS1 enhances inflammasome and caspase-1 activation, we sought to determine whether NS1 directly interacts with inflammasome components. Co-immunoprecipitation experiments showed that NS1 had a strong interaction with caspase-1 in 293T (Fig 3A) and Flag-NS1-inducible THP-1 cells (Fig 3B). Meanwhile, we repeatedly observed an increased protein level of caspase-1 after increasing the effect of NS1 on caspase-1 abundance, and we repeated this work both in THP-1 and in 293T cells. After NS1 overexpression, we observed a considerable accumulation of caspase-1 but not of any other proteins such as IL-1β and NLRP3 (Fig 3C and D). In addition, RT–PCR showed that *caspase-1* mRNA abundance was not altered with NS1 overexpression (Fig 3D). We did not observe the accumulation effect of caspase-1 by DENV-2 NS1 protein, although DENV is a flavivirus closely related to ZIKV (Fig 3E). In line with this result, we observed increased protein abundance of caspase-1 after the infection of both strains of ZIKV but not DENV-2 (Fig EV2D). We next performed cycloheximide (CHX) chase assay to determine whether NS1 affects the stability of caspase-1 (Figs 3F and EV2E) and found that NS1 stabilized caspase-1 protein by delaying its degradation. To reveal which degradation system is responsible for the degradation of caspase-1, we assessed the caspase-1 stability in the presence of different inhibitors and found that NS1-mediated stabilization of caspase-1 was blocked by the proteasome inhibitors MG132, lactacystin, or carfilzomib, but not by the autophagy inhibitor (3MA) or lysosome inhibitor chloroquine (CQ) and NH_4Cl (Figs 3G and EV2F). We also performed confocal microscopy analysis to visualize the co-localization of caspase-1 with the proteasome and observed that caspase-1 co-localized with the proteasome subunit PSMD14. However, the co-localizations were diminished in the presence of NS1, suggesting that the degradation of caspase-1 via proteasome pathway can be inhibited by NS1 (Fig EV2G). Collectively, these results demonstrate that NS1 protects caspase-1 from proteasomal degradation.

Ubiquitination is a major signal for proteasomal degradation. We next analyzed whether NS1 affects the ubiquitination of caspase-1 and found NS1 markedly inhibited the ubiquitination of caspase-1 (Fig 3H). To unravel the possible linkage types affected by NS1, we overexpressed caspase-1 with different types of ubiquitin mutants and found that NS1 markedly inhibited WT and lysine residue 11 (K11)-linked ubiquitination of caspase-1 but had no appreciable effect on the other linkages (Figs 3I and EV2H). These results suggest that NS1 specifically decreases K11-linked poly-ubiquitination of caspase-1, thus preventing its proteasomal degradation.

NS1 recruits USP8 to cleave the K11-linked poly-ubiquitin chains from caspase-1

NS1 is not a deubiquitinase (DUB), so we supposed that NS1 might hijack certain host DUBs to prompt the deubiquitination

Figure 2. NS1 enhances inflammasome activation to benefit ZIKV infection.

A   Relative qRT–PCR analysis of ZIKV RNA in THP-1 cells left untreated or treated with LPS (500 ng/ml, 3 h) and ATP (5 mM, 6 h), followed by ZIKV infection (MOI = 1) for the indicated time points.
B   Relative qRT–PCR analysis of ZIKV RNA in wild type (WT) or NLRP3 knockout (KO) THP-1 cells infected with ZIKV (MOI = 1) for the indicated time points.
C   Immunoblot analysis of extracts of WT or *Nlrp3*$^{-/-}$ BMDMs by the indicated antibodies.
D   Relative qRT–PCR analysis of ZIKV RNA in WT or *Nlrp3*$^{-/-}$ BMDMs infected with ZIKV (MOI = 1) for the indicated time points.
E   Plaque titration of ZIKV in supernatants of WT or *Nlrp3*$^{-/-}$ BMDMs infected with ZIKV (MOI = 1) for the indicated time points.
F   Immunoblot analysis of extracts of WT or caspase-1 KO THP-1 cells by the indicated antibodies.
G   Relative qRT–PCR analysis of ZIKV RNA in WT or caspase-1 KO THP-1 cells infected with ZIKV (MOI = 1) for the indicated time points.
H   Relative qRT–PCR analysis of ZIKV RNA in NS-1-inducible THP-1 cells treated with or without doxycycline (Dox), then left untreated or treated with Ac-YVAD-cmk (20 µM) for 3 h followed by ZIKV infection (MOI = 1) for the indicated time points.
I   Relative qRT–PCR analysis of *NLRP3* knockdown efficiency in PBMCs from two donors.
J   Relative qRT–PCR analysis of ZIKV RNA in PBMCs transfected with control siRNA or *NLRP3* siRNA then infected with ZIKV (MOI = 1) for 36 h.
K   qRT–PCR analysis of ZIKV RNA in PBMCs treated with DMSO or Ac-YVAD-cmk (20 µM) for 3 h followed by ZIKV infection (MOI = 1) for 36 h.

Data information: In (C, F), data are representative of three independent experiments. In (A, B, D, E, G–K), data are mean values ± SEM (n = 3). NS (non-significant), $P > 0.05$; *$P < 0.05$; **$P < 0.01$; ***$P < 0.001$.

of caspase-1 (Nijman *et al*, 2005). To this end, we investigated whether NS1 recruits host DUBs to deubiquitinate thus stabilize caspase-1 in a panel of DUB deficient cells. Among them, we found that knockout of USP8 decreased the stabilization of caspase-1 mediated by NS1 (Figs 4A and EV3A and B). To further corroborate the role of USP8 in NS1-mediated stabilization of caspase-1, we first determined whether USP8 stabilized caspase-1. In line with NS1, USP8 also stabilized caspase-1 by inhibiting its proteasomal degradation, since the stabilization of caspase-1 by USP8 was abrogated by MG132 treatment (Fig 4B).

We next set out to determine the interaction between NS1 and USP8 and found that NS1 could interact with ectopic USP8 (Fig EV3C). Furthermore, we confirmed that NS1 interacted with endogenous USP8 in Flag-NS1-inducible THP-1 cells and the interaction was further enhanced by poly (I:C) transfection (Fig 4C). We next sought to determine whether NS1 functions as a scaffold by recruiting USP8 to caspase-1 and found that the interaction between USP8 and caspase-1 was enhanced by NS1 (Figs 4D and EV3D). We also observed that the interaction between USP8 and caspase-1 was promoted by ZIKV infection in
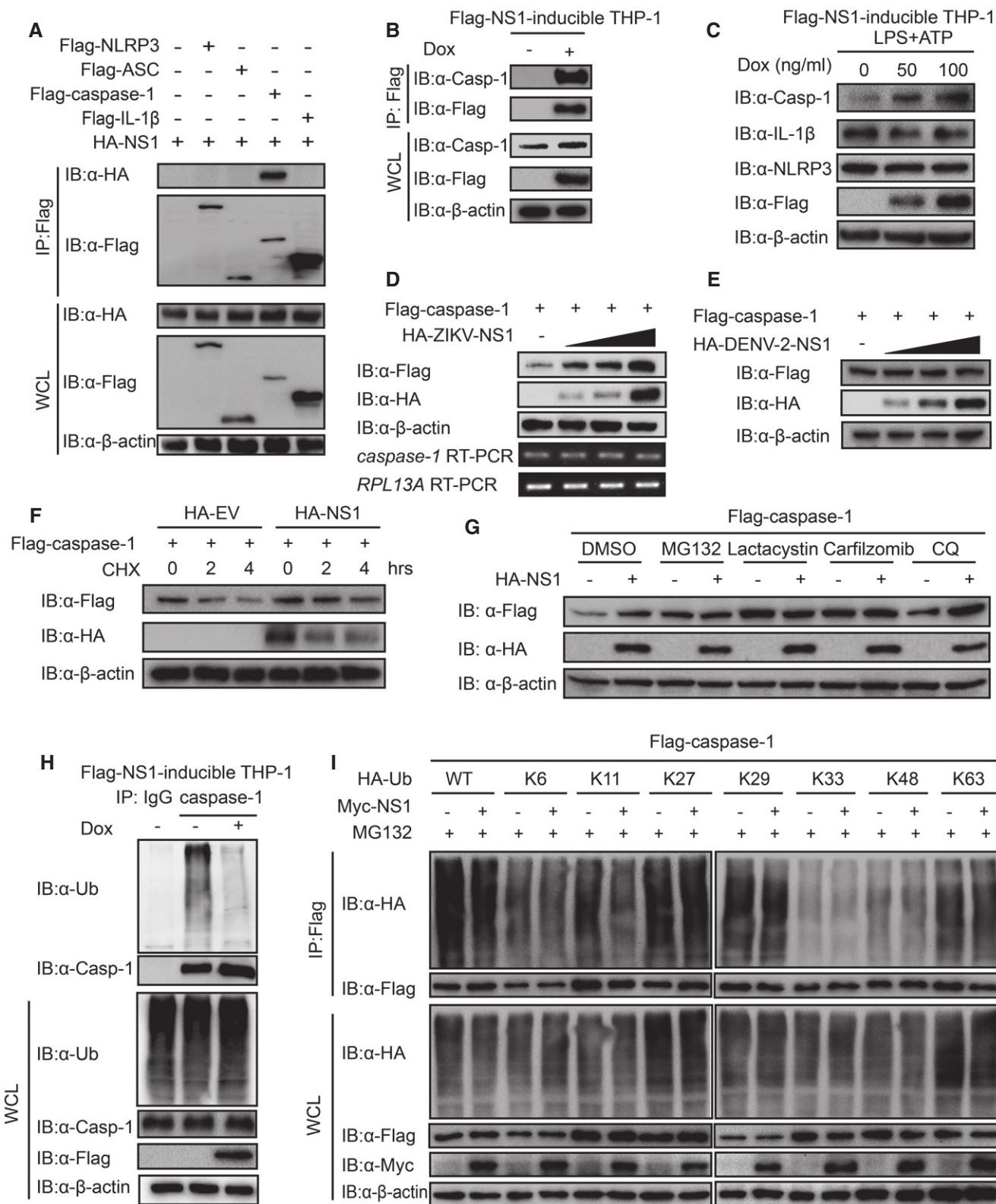
Figure 3.

THP-1 cells (Figs 4E and EV3E). In addition, ZIKV infection failed to enhance the deubiquitination and stabilization of caspase-1 in USP8 KO THP-1 cells (Figs 4F and EV3F).

Moreover, USP8 inhibited total and K11-linked ubiquitination of caspase-1 (Figs 4G and EV3G), which was consistent with the effect of ectopic NS1 (Fig 3I). To further confirm that USP8

Figure 3. NS1 inhibits the proteasomal degradation of caspase-1.

A   Co-immunoprecipitation and immunoblot analysis of extracts of 293T cells transfected with HA-NS1 together with Flag-NLRP3, Flag-ASC, Flag-caspase-1, and Flag-IL-1β. WCL, whole-cell lysates.

B   Co-immunoprecipitation and immunoblot analysis of extracts of NS1-inducible THP-1 cells, which expressed Flag-tagged NS1, treated with or without doxycycline (Dox) (100 ng/ml).

C   Immunoblot analysis of extracts of THP-1 cells treated with LPS (500 ng/ml, 3 h) and ATP (5 mM, 6 h) followed by increasing doses of Dox treatment.

D   Immunoblot analysis of extracts of 293T cells transfected with Flag-caspase-1 together with increasing amount of HA-NS1. Below, *caspase-1* mRNA RT–PCR; *RPL13A* mRNA RT–PCR serves as a loading control.

E   Immunoblot analysis of extracts of 293T cells transfected with Flag-caspase-1 together with increasing amount of HA-DENV-2-NS1.

F   Immunoblot analysis of extracts of 293T cells transfected with Flag-caspase-1 together with empty vector or HA-NS1 followed by cycloheximide (CHX) treatment (100 µg/ml) for the indicated time points. Intensity analysis of the bands from the three independent experiments is shown in Fig EV2E.

G   Immunoblot analysis of extracts of 293T cells transfected with Flag-caspase-1 together with empty vector or HA-NS1 then treated with MG132 (10 mM), lactacystin (5 µM), carfilzomib (100 mM), or CQ (50 mM) for 6 h.

H   Co-immunoprecipitation and immunoblot analysis of extracts of Flag-NS1-inducible THP-1 cells treated with or without Dox (100 ng/ml).

I   Co-immunoprecipitation and immunoblot analysis of extracts of 293T cells transfected with plasmids expressing Flag-caspase-1 and indicated HA-tagged WT ubiquitin or mutants (K6-, K11-, K27-, K29-, K33-, K48-, and K63-only), together with empty vector or Myc-NS1, followed by MG132 (10 mM) treatment for 6 h. Intensity analysis of the bands from the three independent experiments is shown in Fig EV2H.

Data information: Data are representative of three independent experiments.
Source data are available online for this figure.

directly remove the conjugated ubiquitin chains on caspase-1, we performed two-step immunoprecipitation assay. The immunoprecipitates were denatured in SDS-containing lysis and immunoprecipitated again by anti-Flag beads to get rid of un-conjugated ubiquitin chains or other ubiquitinated proteins attached to caspase-1. We found that the ubiquitination of caspase-1 was decreased by NS1 in WT rather than USP8-KO cells (Figs 4H and EV3H), suggesting that USP8 cleaved the conjugated ubiquitin chains on caspase-1 rather than other proteins attached to caspase-1. To further investigate whether deubiquitination of caspase-1 requires the enzyme activity of USP8, we reconstituted USP8 KO cells with WT or enzyme inactive mutant (C786A) (Hasdemir *et al*, 2009) of USP8 and found that USP8-C786A neither inhibited K11-linked ubiquitination of caspase-1 nor stabilized caspase-1, indicating that USP8 affected caspase-1 stability in a protease-dependent manner (Figs 4I and EV3I). Taken together, these results indicate that NS1 recruits USP8 to cleave

K11-linked ubiquitin chains of caspase-1, thus blocking its proteasomal degradation.

NS1-USP8 removes K11-linked poly-ubiquitin Chains from caspase-1 on Lys134

To identify the lysine residues of caspase-1 to which K11-linked ubiquitin is attached, we performed an *in silico* search for ubiquitin binding sites on caspase-1 using the UbPred program (Radivojac *et al*, 2010). This analysis revealed seven putative target lysine residues: K11, K37, K44, K64, K134, K296, and K319. We then generated Flag-caspase-1 mutants in which each of these lysine residues was replaced with arginine (R) and found that NS1 failed to stabilize caspase-1-K134R mutant, but not other caspase-1 mutants (Figs 5A and EV3J). Ubiquitination assay also revealed that caspase-1-K134R mutant displayed a dramatic reduction of K11-linked ubiquitination (Fig 5B). The

Figure 4. NS1 recruits USP8 to cleave K11-linked poly-ubiquitin chains from caspase-1.

A   Immunoblot analysis of extracts of wild type (WT) and USP8 knockout (KO) 293T cells transfected with Flag-caspase-1 together with empty vector or Myc-NS1.

B   Immunoblot analysis of extracts of transfected with Flag-caspase-1 together with empty vector or Myc-USP8 then treated with or without MG132 (10 mM) for 6 h.

C   Co-immunoprecipitation and immunoblot analysis of extracts of Flag-NS1-inducible THP-1 cells treated with or without Dox (100 ng/ml) then transfected with or without poly (I:C) (2 mg/ml, 6 h).

D   Co-immunoprecipitation and immunoblot analysis of extracts of 293T cells transfected with Flag-caspase-1 and Myc-USP8 together with HA-NS1 followed by MG132 treatment (10 mM) for 6 h. Intensity analysis of the bands from the three independent experiments is shown in Fig EV3D.

E   Co-immunoprecipitation and immunoblot analysis of extracts of THP-1 cells infected with ZIKV (MOI = 1) for 24 h. Intensity analysis of the bands from the three independent experiments is shown in Fig EV3E.

F   Co-immunoprecipitation and immunoblot analysis of extracts of WT and USP8 KO THP-1 cells infected with ZIKV (MOI = 1) for 24 h. Intensity analysis of the bands from the three independent experiments is shown in Fig EV3F.

G   Co-immunoprecipitation and immunoblot analysis of extracts of 293T cells transfected with plasmids expressing Flag-caspase-1 and indicated HA-tagged WT ubiquitin (Ub) or mutants (K6-, K11-, K27-, K29-, K33-, K48-, and K63-only), together with empty vector or Myc-USP8, followed by MG132 (10 mM) treatment for 6 h. Intensity analysis of the bands from the three independent experiments is shown in Fig EV3G.

H   Immunoblot analysis of extracts of WT or USP8 KO 293T cells transfected with Flag-caspase-1, HA-K11-Ub together with empty vector or Myc-NS1, followed by two-step immunoprecipitation with anti-Flag beads and immunoblot analysis with anti-HA. Intensity analysis of the bands from the three independent experiments is shown in Fig EV3H.

I   Co-immunoprecipitation and immunoblot analysis of extracts of USP8 KO 293T cells transfected with Flag-caspase-1 and HA-K11-Ub together with WT or inactive mutant C786A of USP8. Intensity analysis of the bands from the three independent experiments is shown in Fig EV3I.

Data information: Data are representative of three independent experiments.
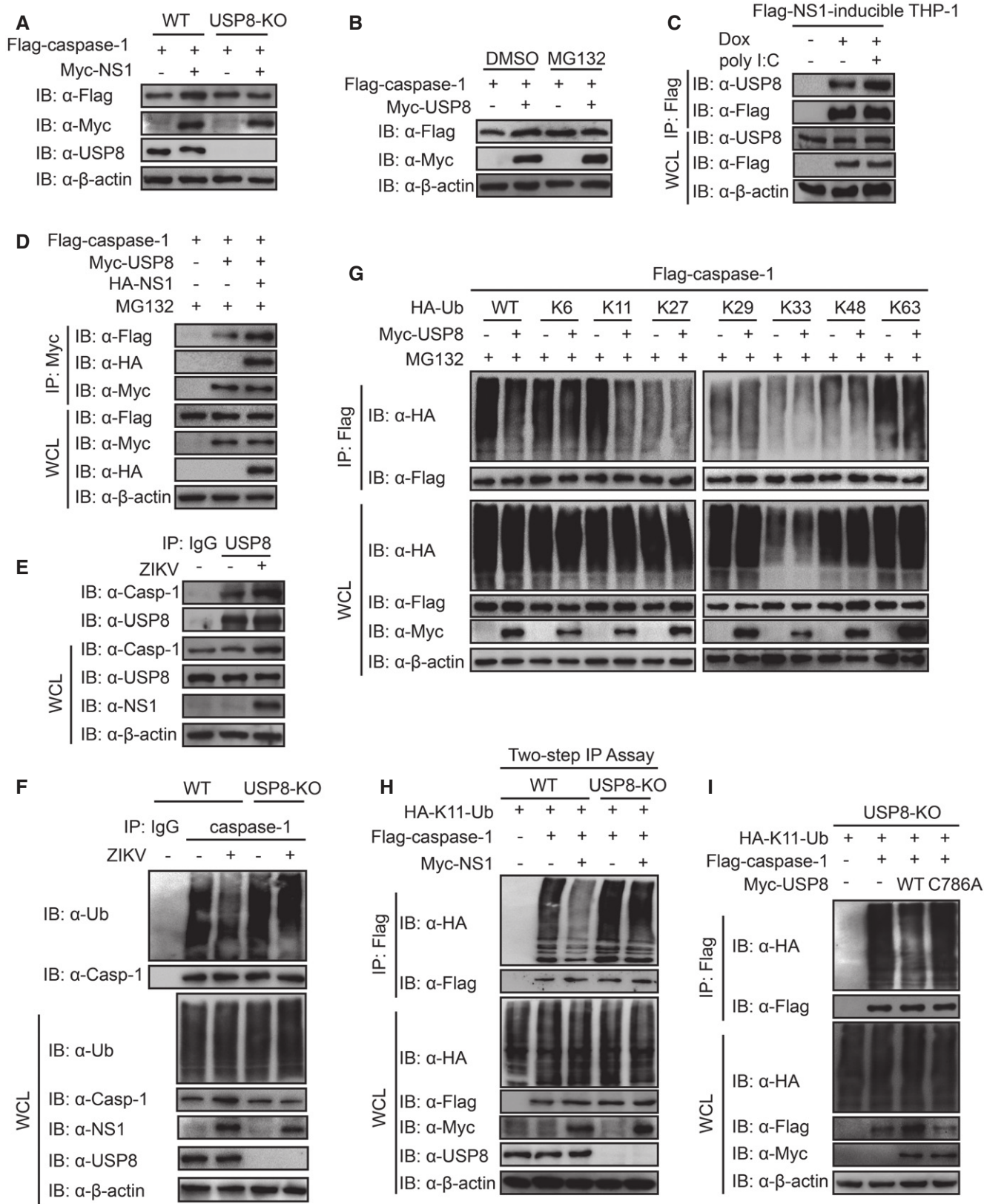Source data are available online for this figure.
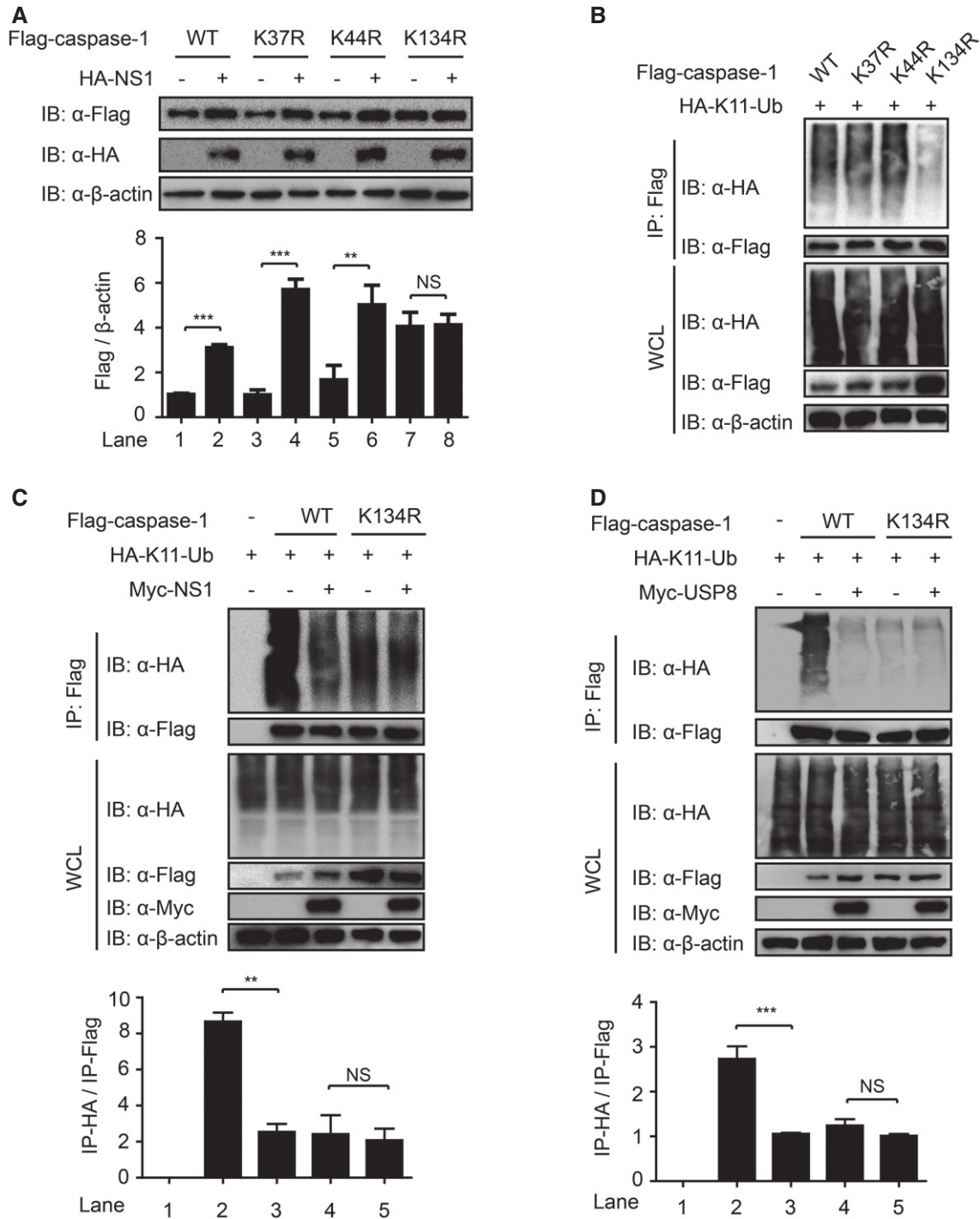
Figure 4.

Figure 5.   NS1 stabilizes caspase-1 through the cleavage of poly-ubiquitin chains at Lys134.

A   Immunoblot analysis of extracts of 293T cells transfected with empty vector or HA-NS1 together with Flag-caspase-1 wild type (WT) and mutants (K37R, K44R, or K134R). Lower panel shows the intensity analysis of the bands from the three independent experiments. K11R, K64R, K296R, and K319R are shown in Fig EV3J.

B   Co-immunoprecipitation and immunoblot analysis of extracts of 293T cells transfected with HA-K11-ubiquitin (Ub) together with Flag-caspase-1 (WT, K37R, K44R, K134R).

C   Co-immunoprecipitation and immunoblot analysis of extracts of 293T cells transfected with Flag-caspase-1 (WT or K134R) and HA-K11-Ub, together with empty vector or Myc-NS1. Lower panel shows the intensity analysis of the bands from the three independent experiments.

D   Co-immunoprecipitation and immunoblot analysis of extracts of 293T cells transfected with Flag-caspase-1 (WT or K134R) and HA-K11-Ub, together with empty vector or Myc-USP8. Lower panel shows the intensity analysis of the bands from the three independent experiments.

Data information: Data are representative of three independent experiments. In (A, C, D), data are mean values ± SEM ($n = 3$). NS (non-significant), $P > 0.05$; **$P < 0.01$; ***$P < 0.001$.

Source data are available online for this figure.

caspase-1-K134R mutant seemed to be more stable than the WT protein. It is due to that K134R abolished the ubiquitination on this site, thus blocking its degradation. We next found NS1 and USP8 failed to decrease the K11-linked ubiquitination of K134R (Fig 5C and D). Moreover, we found that the K11-linked ubiquitination of WT caspase-1 was further decreased when NS1 and USP8 were co-expressed, while K11-linked ubiquitination of caspase-1-K134R mutant was not affected by either NS1 or USP8 (Fig EV3K and L). These results suggest that NS1-USP8 specifically removes the K11-linked poly-ubiquitin chains from caspase-1 on Lys134.

NS1-mediated inflammasome activation attenuates type I IFN signaling *in vitro* and *in vivo*

Caspase-1 has been characterized to play central roles in the fine-tuning regulation between type I IFN and inflammasome activation (Winkler & Rosen-Wolff, 2015). Considering the vital antiviral effect of type I IFN against ZIKV, we wondered whether NLRP3 inflammasome activation affects type I IFN signaling during ZIKV infection. We found that the expression of IFN-β and its downstream interferon stimulated genes (ISGs), including IFIT1 and IFIT2, was stronger in caspase-1 KO THP-1 cells, compared to that in WT THP-1 cells after ZIKV infection (Fig 6A). Consistently, we observed that ZIKV induced lower type I IFN response in THP-1 cells pre-treated with LPS plus ATP, compared to the un-pre-treated group (Fig 6B). NLRP3 is indispensable for ZIKV-mediated caspase-1 activation (Fig 1C), and we found that the expression of IFN-β was much higher in NLRP3 KO cells than in WT THP-1 cells during ZIKV infection (Fig 6C). Meanwhile, we observed this phenomenon after the infection of both strains of ZIKV (Fig EV4A). We next found that the inhibition of type I IFN by overexpressing NS1 was largely rescued by YVAD treatment (Fig 6D). Furthermore, knockdown of *NLRP3* in PBMCs promoted the expression of IFN-β (Fig 6E). YVAD treatment also facilitated the transcription and secretion of IFN-β in PBMCs (Fig 6F and G), which were consistent with our observations in THP-1 cells. Collectively, ZIKV-induced type I IFN production was attenuated by NS1-mediated NLRP3 inflammasome activation, which led to higher viral replication (Fig 2).

To further address the impact of inflammasome activation on type I IFN signaling, we performed *in vivo* ZIKV infection in $Nlrp3^{-/-}$ mice. According to previous work, 1-day-old neonatal mice were intracerebrally injected with ZIKV for 5 days (Manangeeswaran *et al*, 2016; Shan *et al*, 2017). The production of IL-1β was significantly decreased in the brains of $Nlrp3^{-/-}$ mice than that in WT mice (Fig 6H). We detected a prominent increase in the production of IFN-β in the brains from $Nlrp3^{-/-}$ mice, compared to that from WT mice, after ZIKV infection (Fig 6I and J). Meanwhile, lower accumulation of viral RNA as well as ZIKV infectivity titers in the brain of $Nlrp3^{-/-}$ mice was observed (Fig 6K and L). Additionally, $Nlrp3^{-/-}$ mice showed a higher rate of weight gain than WT mice after ZIKV infection (Fig 6M). Together, ZIKV takes advantage of the inflammasome activation to impose restrictions on type I IFN signaling, thus facilitating its replication both *in vitro* and *in vivo*.

Cleavage of cGAS by caspase-1 assists ZIKV replication

Previous study demonstrates caspase-1 could cleave cGAS during DNA virus infection (Wang *et al*, 2017). To test whether NS1-mediated stabilization of caspase-1 can attenuate type I IFN signaling through cGAS, we infected Flag-NS1-inducible THP-1 cells with HSV-1 (a DNA virus) and observed a significant inhibition of type I IFN signaling when NS1 was expressed (Fig EV4B). To evaluate the function of cGAS during ZIKV infection, we constructed cGAS KO cell line (Fig EV4C) and detected an increased ZIKV replication (Fig 7A) and decreased host resistance in the absence of cGAS (Fig 7B), indicating that cGAS plays a critical role in the defense of ZIKV. Furthermore, we examined the role of cGAS in PBMCs during ZIKV infection. Knockout of *cGAS* also facilitated ZIKV replication and impaired IFN-β production, while knockout of *NLRP3* showed the opposite effect (Figs 7C and EV4D). To prove the effect of inflammasome activation on type I IFN and ZIKV replication is dependent on cGAS, we examined whether the function of inflammasome to prompt ZIKV infection still exists in the absence of cGAS. As expected, both YVAD (Fig 7D) and LPS plus ATP (Fig EV4E) lost their effects to benefit ZIKV replication in cGAS KO cells. In line with that, ectopic cGAS was cleaved in THP-1 cells after infection with either HSV-1 or ZIKV, and the cleavage of cGAS was not detected in the presence of YVAD (Fig 7E), suggesting ZIKV infection induced cGAS cleavage by caspase-1. We also detected the abundance of cGAS after ZIKV infection in NLRP3 KO and caspase-1 KO THP-1 cells and found that NLRP3 and caspase-1 deficiency resulted in higher abundance of endogenous cGAS (Fig 7F and G). These observations were further confirmed in WT and $Nlrp3^{-/-}$ BMDMs, and we detected enhanced phosphorylation of TBK1 and IRF3 in $Nlrp3^{-/-}$ BMDMs during ZIKV infection (Fig 7H). In human primary cells, knockdown of *NLRP3* also resulted in the accumulation of cGAS (Fig 7I). Furthermore, we found that NS1 stabilized pro-caspase-1 and produced more active caspase-1, which in turn promoted the cleavage of cGAS (Fig 7J). We next reconstituted cGAS KO THP-1 cells with WT or D140A/D157A cGAS mutant, which cannot be cleaved by caspase-1, and found that compared to WT cGAS, cGAS D140A/D157A mutant generated stronger antiviral responses upon ZIKV infection (Figs 7K and EV4F), firmly proving the connection between the cleavage of cGAS with the inhibition of type I IFN during ZIKV infection.

As a DNA sensor, cGAS is also reported to be involved in the detection of some RNA viruses, such as DENV, through recognizing mitochondrial DNA (mtDNA) as a ligand (Aguirre *et al*, 2017). To test whether mtDNA could also induce type I IFN responses through cGAS during ZIKV infection, we evaluated the relative abundance of genomic DNA (gDNA) versus mtDNA in samples with or without ZIKV infection. We found the gDNA fragments bound to cGAS exhibited no significant differences after ZIKV infection, while the mtDNA bound to cGAS showed an enrichment for four mtDNA fragments in ZIKV-infected cells (Fig EV4G and H), demonstrating that mtDNA is enriched and is bound to cGAS during ZIKV infection. In conclusion, ZIKV infection induced a release of mtDNA which was identified as a ligand for cGAS.

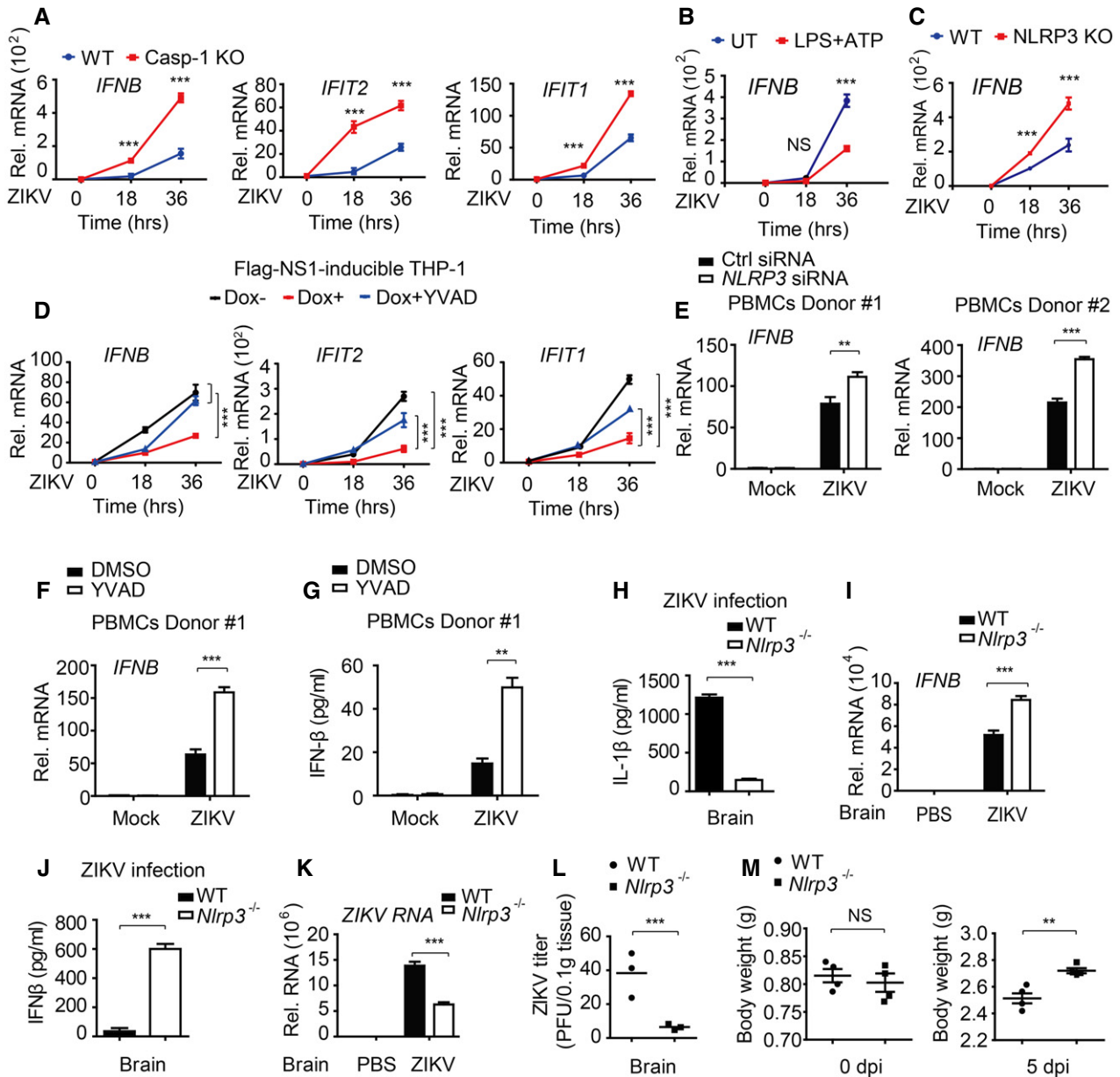Although both ZIKV and DENV target cGAS for immune evasion, they use different strategies. DENV directly degraded

Figure 6. NS1-mediated NLRP3 inflammasome activation attenuates type I IFN signaling.

A Relative qRT–PCR analysis of *IFNB*, *IFIT2*, and *IFIT1* mRNA levels in wild type (WT) or caspase-1 knockout (KO) THP-1 cells infected with ZIKV (MOI = 1) for the indicated time points.

B Relative qRT–PCR analysis of *IFNB* mRNA levels in THP-1 cells left untreated or treated with LPS (500 ng/ml, 3 h) and ATP (5 mM, 6 h), followed by ZIKV infection (MOI = 1) for the indicated time points.

C Relative qRT–PCR analysis of *IFNB* mRNA levels in wild type (WT) or NLRP3 knockout (KO) THP-1 cells infected with ZIKV (MOI = 1) for the indicated time points.

D Relative qRT–PCR analysis of *IFNB*, *IFIT2*, and *IFIT1* mRNA levels in Flag-NS1-inducible THP-1 cells treated with or without Dox then left untreated or treated with YVAD (20 μM) for 3 h, followed by ZIKV infection (MOI = 1) for the indicated time points.

E Relative qRT–PCR analysis of *IFNB* mRNA in PBMCs transfected with control siRNA or *NLRP3* siRNA then infected with ZIKV (MOI = 1) for 36 h.

F Relative qRT–PCR analysis of *IFNB* mRNA in PBMCs treated with DMSO or Ac-YVAD-cmk (20 μM) for 3 h followed by ZIKV infection (MOI = 1) for 36 h.

G ELISA of IFN-β in the supernatants of PBMCs treated with DMSO or Ac-YVAD-cmk (20 μM) for 3 h followed by ZIKV infection (MOI = 1) for 36 h.

H ELISA of IL-1β production in brain of WT or $Nlrp3^{-/-}$ 1-day-old neonatal mice ($n = 3$ per group) intracerebrally injected with 1×10^5 plaque-forming units (PFU) of ZIKV for 5 days.

I Relative qRT–PCR analysis of *IFNB* mRNA levels in brain tissues of WT or $Nlrp3^{-/-}$ neonatal mice with or without ZIKV infection in panel (H).

J ELISA of IFN-β production in brains of WT or $Nlrp3^{-/-}$ neonatal mice in (H).

K Relative qRT–PCR analysis of ZIKV RNA levels in brain tissues of WT or $Nlrp3^{-/-}$ neonatal mice with or without ZIKV infection in (H).

L Plaque titration of ZIKV in brain tissues of WT or $Nlrp3^{-/-}$ neonatal mice shown in (H).

M Body weight gain of WT and $Nlrp3^{-/-}$ neonatal mice ($n = 4$ per group) inoculated with ZIKV (1×10^5 PFUs).

Data information: Data are mean values ± SEM ($n = 3$). NS (non-significant), $P > 0.05$; **$P < 0.01$; ***$P < 0.001$.
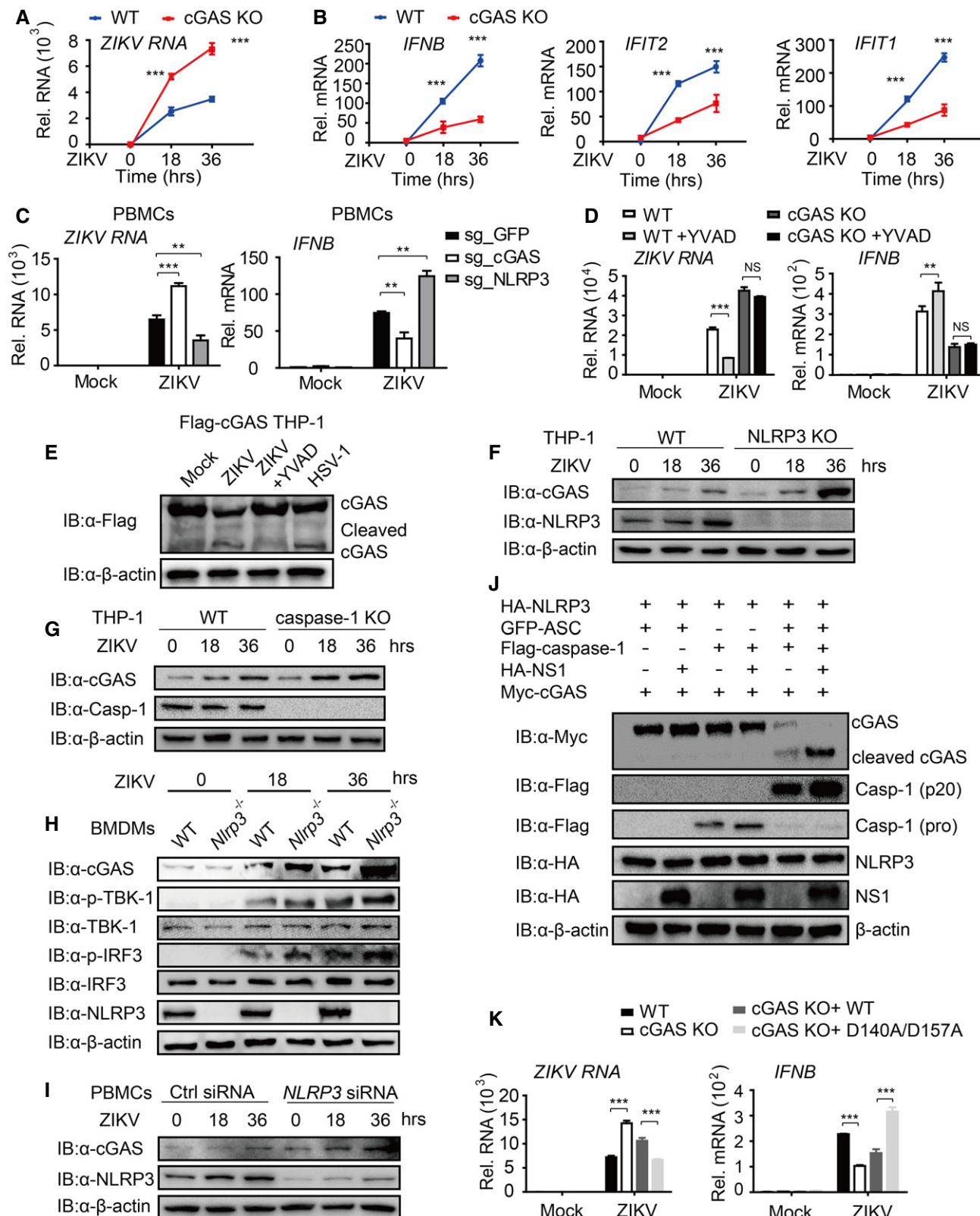
Figure 7.

cGAS by NS2B while ZIKV promoted the cleavage of cGAS via inflammasome activation. NS1 of ZIKV alone has no effect on cGAS (Fig EV4I). Taken all data together, we conclude that the

stabilization of caspase-1 by NS1 assists ZIKV replication through the cleavage of cGAS to antagonize type I IFN signaling (Fig 8).

Figure 7. Cleavage of cGAS by caspase-1 inhibits type I IFN signaling and assists ZIKV replication.

A   Relative qRT–PCR analysis of ZIKV RNA levels in wild type (WT) or cGAS knockout (KO) THP-1 cells after ZIKV infection (MOI = 1) for indicated time points.

B   Relative qRT–PCR analysis of *IFNB*, *IFIT2*, and *IFIT1* mRNA levels in WT or cGAS KO THP-1 cells after ZIKV infection (MOI = 1) for indicated time points.

C   Relative qRT–PCR analysis of ZIKV RNA and *IFNB* mRNA levels in PBMCs transduced with Cas9 and small-guide RNA targeting GFP, cGAS, or NLRP3 and infected with ZIKV (MOI = 1) for 36 h.

D   Relative qRT–PCR analysis of ZIKV RNA and *IFNB* mRNA levels in WT or cGAS KO THP-1 cells treated with or without YVAD (20 μM), followed by ZIKV infection (MOI = 1) for indicated times points.

E   Immunoblot analysis of extracts of Flag-cGAS-overexpressed THP-1 cells treated with or without YVAD (20 μM) then infected with ZIKV (MOI = 5) for 24 h or infected with HSV-1 (MOI = 1) for 24 h.

F, G   Immunoblot analysis of WT, NLRP3 KO (F), and caspase-1 KO (G) THP-1 cells infected with ZIKV (MOI = 1) for the indicated time points.

H   Immunoblot analysis of extracts of WT or *Nlrp3*$^{-/-}$ BMDMs infected with ZIKV (MOI = 1) for the indicated time points.

I   Immunoblot analysis of PBMCs from Donor #1 transfected with control siRNA or *NLRP3* siRNA followed by ZIKV infection (MOI = 1) for the indicated time points.

J   Immunoblot analysis of extracts of 293T cells transfected with Myc-cGAS (tagged on C-terminal), GFP-ASC, Flag-caspase-1, together with empty vector or HA-NS1.

K   Relative qRT–PCR analysis of ZIKV RNA and *IFNB* mRNA levels in WT, cGAS KO THP-1 cells, as well as cGAS KO THP-1 cells reconstituted with WT or D140A/D157A mutant of cGAS, followed by ZIKV infection (MOI = 1) for 24 h. Expression levels of restored cGAS WT or D140A/D157A mutant were determined by immunoblot analysis in Fig EV4F.

Data information: In (E–J), data are representative of three independent experiments. In (A–D, K), data are mean values ± SEM (*n* = 3). NS (non-significant), *P* > 0.05; ****P* < 0.01; ***P* < 0.001.

Source data are available online for this figure.

Discussion

The host innate immune system triggers its activity through multiple ways to carry out the task of antiviral process. Both type I IFN and inflammasome signaling are indispensable in response to viral infection (Akira *et al*, 2006). Virus recognition triggers transcriptional activation of cytokines and type I IFN responsive genes (Schneider *et al*, 2014), while the formation of inflammasomes enables proteolytic activation of caspase-1, which in turn can cleave multiple pro-inflammatory substrates including pro-IL-1β and pro-IL-18 (Martinon *et al*, 2009). Cell inherent antiviral effector proteins exert their functions by targeting different viral components in every period of viral life history (Schneider *et al*, 2014). It is thus no surprising that viruses have evolved an array of sophisticated strategies to counteract host immune response (Fernandez-Garcia *et al*, 2009). For example, NS1 of influenza antagonizes type I IFN signaling by targeting RIG-I (Gack *et al*, 2009); DENV, another member of *Flavividae* family, mediates a drastic degradation of cGAS by its protease cofactor NS2B (Aguirre *et al*, 2017). Distinct from other *Flaviviridae* family members directly targeting and inhibiting the cytosolic signaling molecules (Fernandez-Garcia *et al*, 2009; Chan & Gack, 2016; Aguirre *et al*, 2017), ZIKV has come up with a more dramatic strategy. In this report, we identify a novel mechanism that ZIKV utilizes the inflammasome activation to suppress type I IFN signaling thus assisting its replication. After ZIKV infection, NS1 recruits USP8 to cleave the K11-linked poly-ubiquitin chains from caspase-1 at Lys134, thus stabilizing caspase-1 to enhance inflammasome activation. The active caspase-1 in turn promotes the cleavage of cGAS, which recognizes mtDNA to initiate type I IFN signaling during ZIKV infection. Finally, type I IFN production is attenuated and ZIKV evades host antiviral response (Fig 8).

Recent studies indicate that cGAS-mediated type I IFN signaling is an essential component of host antiviral immunity (Chen *et al*, 2016). Although cGAS has been classified as a DNA sensor, it has also been demonstrated to have antiviral effect against several RNA viruses, including DENV and other members of flavivirus family (Schoggins *et al*, 2014). A recent study demonstrates that cGAS restricts DENV replication through sensing mitochondrial damage (Aguirre *et al*, 2017). Here, we also show that cGAS is critical to the antiviral defense of ZIKV, and we observed the mtDNA recognition

by cGAS during ZIKV infection, suggesting that prevalent mitochondrial dysfunction may be a shared feature during flavivirus infection.

In order to evade cGAS-mediated viral detection, ZIKV employs several elaborate mechanisms to cleave and remove the intracellular cGAS. On the first step, ZIKV NS1 recruits USP8 to maintain the stabilization of caspase-1. Since caspase-1 is a unique cysteine protease playing central roles in innate immunity (Shrivastava *et al*, 2016), the stability and activation of caspase-1 should be controlled strictly. While the K63-linked ubiquitination is responsible for the activation of caspase-1 (Labbe *et al*, 2011), our study demonstrates that the K11-linked ubiquitination of caspase-1 is a signal to induce its proteasomal degradation, and this process can be reversed by the deubiquitinase USP8. Utilizing this endogenous stabilization mechanism of caspase-1, ZIKV hijacks USP8 to enhance pro-caspase-1 abundance in the cytoplasm. Secondly, high abundance of active caspase-1 produced through ZIKV-induced NLRP3 inflammasome activation leads to the cleavage and removal of cGAS, which in turn enhances the replication of ZIKV. Different from previous studies, which have shown that a number of viruses encode proteins directly targeting to inflammasome components to impede inflammasome activation (Taxman *et al*, 2010), we found that ZIKV manages to evade cGAS-mediated detection by benefiting from caspase-1-dependent inflammasome activation.

Besides the well-known pro-inflammatory functions in processing pro-IL-1β and pro-IL-18, or promoting inflammasome-induced pyroptosis, caspase-1 has now been identified to play additional roles in antiviral immune response by fine-tuning the expression of antiviral cytokines (Wang *et al*, 2017). Regulation of type I IFN signaling and autophagy by caspase-1 is mediated by the cleavage of TIR-domain-containing adapter inducing interferon-β (TRIF) (Jabir *et al*, 2014). Picornavirus has come up with a more dramatic strategy to trigger MDA5 and RIG-I cleavage and degradation by using host caspases (Barral *et al*, 2009). Accumulating evidence from other groups revealed that inflammasome activation is necessary during ZIKV infection (Khaiboullina *et al*, 2017; Wang *et al*, 2018). Our *in vivo* experiments also suggest that NLRP3 inflammasome deficiency protects mice from ZIKV infection. Taken together, instead of pathogen clearance, inflammasome activation plays a "villain" against type I IFN antiviral response during ZIKV infection.
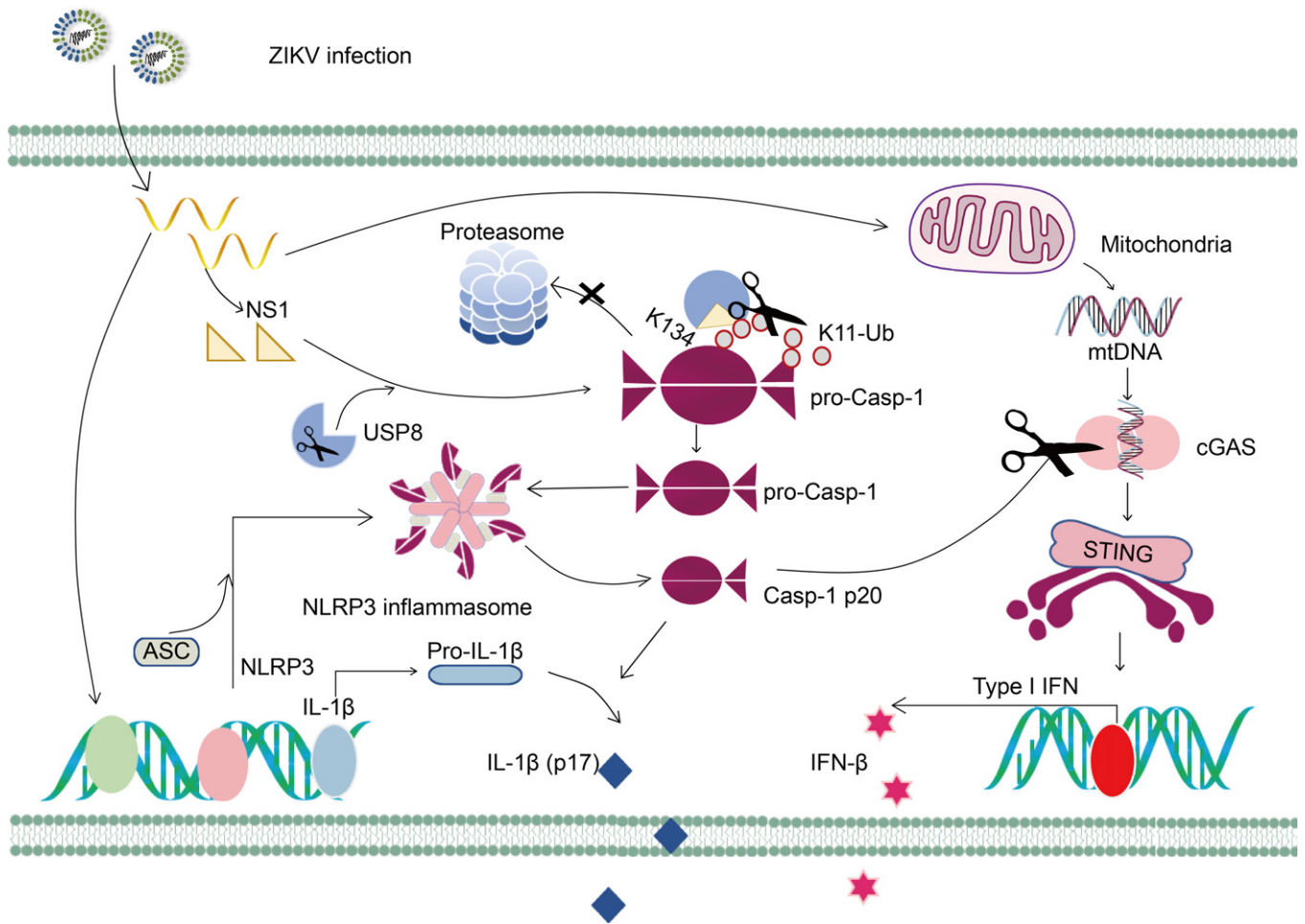
Figure 8. Schematic representation of ZIKV by targeting the cross-talk between inflammasome and type I IFN signaling.

ZIKV non-structural proteins NS1 enhance inflammasome activation to benefit its infection by recruiting USP8 to cleave K11-linked poly-ubiquitin chains from caspase-1 at Lys134. NS1-mediated stabilization of caspase-1 further promotes the cleavage of cGAS, thus inhibiting type I IFN signaling as well as antiviral innate immunity.

ZIKV detection by cGAS is due to virus-induced release of host-derived immune-stimulatory danger signals and the induction of type I IFN is a critical part of host antiviral defense to ZIKV. To evade host defense, ZIKV craftily targets to the antagonistic mechanisms between NLRP3 inflammasome and type I IFN pathways, in which caspase-1 activated by inflammasome cleaves cGAS. Further studies are required to unravel the interplay between inflammasome and type I IFN during different kinds of viral infection.

ZIKV exhibits strong neurotropism and has strong links with the incidence of microcephaly (Rubin *et al*, 2016). It has been implied that ZIKV might cross the placenta by utilizing monocytes as a carrier (Khaiboullina *et al*, 2017). Here, we demonstrate a detailed mechanism that ZIKV utilized to enhance its replication in the monocyte-derived cells, thus contributing to its transmission and pathogenesis. That might be the reason why NS1 promotes instead of suppressing inflammasome activation. We also highlight the important role of caspase-1, as the hub of two most important antiviral pathways, which is skillfully used by ZIKV to assist its infection and transmission. Pharmacological inhibition of caspases has been shown to be a potential therapeutic approach for a series of diseases in several animal models and clinical trials (Lee *et al*,

2018). Given the importance of caspase-1 in ZIKV infection, it is of great potential to develop novel strategies or inhibitors targeting caspase-1, and even USP8, for the therapy of ZIKV infection. In summary, our study unveils a novel mechanism by which ZIKV manipulates the cross-talk of inflammasome and type I IFN signaling to evade antiviral response, which might suggest a framework for rational vaccine design and antiviral development.

Materials and Methods

Cell lines and cultures

Human embryonic kidney cells (HEK293T) from ATCC and African green monkey kidney epithelial cells (Vero) from ATCC were cultured in DMEM (Corning) with 10% fetal bovine serum (GenStar). THP-1 cells from ATCC and bone marrow-derived macrophages (BMDMs) were maintained in RPMI-1640 medium (Gibco) with 10% fetal bovine serum in a 5% CO_2 incubator at 37°C. Blood from healthy donors was used for the isolation of PBMCs by Ficoll–Hypaque density-gradient centrifugation. The use of PBMCs was in compliance

with institutional ethics guidelines and approved protocols of Sun Yat-sen University. The cell lines were tested for mycoplasma contamination by MycoAler Mycoplasma Detection Kit (Lonza).

Antibodies and reagents

Horseradish peroxidase (HRP)-anti-Flag (M2) (A8592), anti-β-actin (A1978) were purchased from Sigma. Anti-hemagglutinin-HRP (HA) (3F10) and mouse monoclonal anti-c-Myc-HRP (11814150001) were purchased from Roche Applied Science. Anti-caspase-1 (#2225), anti-IL-1β (3A6), anti-pTBK1 (S172) (#5483P), anti-TBK1 (#3504), anti-pIRF3 (S396) (#4947), anti-PSMD14 (#4197) were acquired from Cell Signaling Technology. Anti-cGAS (sc-24558), anti-IRF3 (sc-33641), anti-Ub (sc-8017), anti-USP8 (sc-376130) were purchased from Santa Cruz Biotechnology. Anti-AIM2 (#ab93015) was purchased from Abcam. Rabbit polyclonal antibodies against murine cGAS (R3252-1) were from Abiocode. Anti-NLRP3 (#A27391510) was from AdipoGen. Mouse and rabbit IgG were from Beyotime. Protein G agarose and protein A agarose were purchased from Pierce.

Lipopolysaccharide (LPS), MG132 (C-2211-5MG), doxycycline (Dox; D9891), chloroquine phosphate (CQ) (PHR1258-1G), and 3-methyladenine (3-MA) (M9281-100MG) were purchased from Sigma. Lactacystin and carfilzomib were purchased from ApexBio. ATP and poly(I:C) (LMW) were purchased from Invivogen. Ac-YVAD-cmk (10014) was purchased from Cayman Chemical Company.

Viruses and plasmids

ZIKV GZ01 (KU820898) and ZIKV (UG MR766) strains (Schwarz *et al*, 2016) are used in this study. It is GZ01 if not specified. Herpes simplex virus type 1 (HSV-1, KOS strain) was kindly provided by Dr. Guoying Zhou, Guangzhou Medical University. Plaque assays were performed to determine viral titer as previously described (Wu *et al*, 2017). Cells were infected at various MOI, as previously described (Wu *et al*, 2017). Plasmids encoding NS1, NS2B3, and NS4B of ZIKV were previously described (Wu *et al*, 2017). Other plasmids mentioned were acquired by the means of standard PCR techniques.

Mice and animal study

C57BL/6 *Nlrp3*$^{-/-}$ mice were kindly provided by Dr. Rongbin Zhou, University of Science and Technology of China. C57BL/6 WT mice were purchased from Guangdong Medical Laboratory Animal Center. Mice were kept and bred in specific-pathogen-free (SPF) conditions and were randomly chosen for experiments. The Institutional Animal Care and Use Committee of Sun Yat-sen University, PRC, approved all the experimental protocols concerning the handling of mice. The isolation of BMDMs was performed as described previously (Chen *et al*, 2016). For *in vivo* infection of ZIKV, 1-day-old WT and *Nlrp3*$^{-/-}$ C57BL/6 neonatal mice were injected with PBS or 1×10^5 PFU ZIKV intracerebrally. RNA levels, cytokine productions, and virus infectivity titer in brain were analyzed at 5 days post-infection.

Immunoprecipitation and immunoblot analysis

For immunoprecipitation, whole-cell extracts were prepared after transfection or stimulation with appropriate ligands, followed by incubation overnight with the appropriate antibodies plus Protein A/G beads. For immunoprecipitation with anti-Flag or anti-HA, anti-Flag, or anti-HA agarose gels (Sigma) were used. Beads were then washed five times with low-salt lysis buffer (50 mM HEPES, 150 mM NaCl, 1 mM EDTA, 10% glycerol, 1.5 mM MgCl$_2$, and 1% Triton X-100), and immunoprecipitates were eluted with $2 \times$ SDS loading buffer and resolved by SDS–PAGE. Proteins were transferred to PVDF membranes (Bio-Rad) and further incubated with the appropriate antibodies. Immobilon Western Chemiluminescent HRP Substrate (Millipore) was used for protein detection.

Two-step immunoprecipitation and ubiquitination assays

Two-step immunoprecipitation and ubiquitination assays were performed according to the previous report (Wang *et al*, 2014). For the first-step immunoprecipitation assay, whole-cell extracts were prepared by using low-salt buffer supplemented with a 5 mg/ml protease inhibitor cocktail (Roche). Lysates were incubated with the anti-Flag beads overnight. The immunoprecipitates were washed 3–5 times with low-salt buffer. For the second-step immunoprecipitation assay, the immunoprecipitates were denatured by boiling for 5 min in the lysis buffer containing 1% SDS. The elutes were diluted 1:10 with low-salt buffer. The diluted elutes were reimmunoprecipitated with anti-Flag beads overnight. After 3–5 times wash, the immunoprecipitates were resolved by SDS–PAGE.

Gene edition by CRISPR/Cas9 technology

After 293T, THP-1 cells, and PBMCs were seeded, medium was replaced with DMEM containing polybrene (8 μg/ml) (Sigma) and lentiviruses expressing Cas9 and specific sgRNAs for 18 h. Cells were selected for puromycin resistance, and polyclonal pools of transduced cells were used for clonal selection and following experiments. The small-guide RNA (sgRNA) sequences targeting indicated genes are as follows:

GFP guide RNA: 5′-CACCGGGGCGAGGAGCTGTTCACCG-3′
NLRP3 guide RNA: 5′-AAGGAAGAAGACGTACACCG-3′
caspase-1 guide RNA: 5′-TCCACTAGCATCTTACCTTG-3′
AIM2 guide RNA: 5′-CCTTATCCTACCTTAACATG-3′
cGAS guide RNA: 5′-CGGCCCCCATTCTCGTACGG-3′
USP4 guide RNA: 5′-ATGAGGACCACACTCCAACG-3′
USP6 guide RNA: 5′-AGATGACACGAACGAGCAAG-3′
USP8 guide RNA: 5′-ATGCAGATTAGATCGTGATG-3′
USP10 guide RNA: 5′-GCCTGGGTACTGGCAGTCGA-3′
USP14 guide RNA: 5′-GAATGACTCTACTAATGATG-3′
USP18 guide RNA: 5′-CTGCGAGGACTCAGCCAGGA-3′
USP25 guide RNA: 5′-AGTTGTCTCCTCCTGCTGAG-3′
USP27 guide RNA: 5′-ACAAGCCTCCACCTCAACAG-3′
USP31 guide RNA: 5′-TGGACAGCGTCTTGAGAACG-3′
USP32 guide RNA: 5′-GATCGGATTCCTCAGCTACG-3′

RNA extraction and quantitative RT–PCR

Total RNA was extracted using TRIzol reagent (Invitrogen) and reverse-transcribed using oligo-dT primers and reverse transcriptase (Vazyme). Real-time quantitative PCR was performed using SYBR Green qPCR Mix kit (GenStar) with the primers listed below:

Human IFN-β: forward: 5′-CCTACAAAGAAGCAGCAA-3′
Reverse: 5′-TCCTCAGGGATGTCAAAG-3′
Human IFIT2: forward: 5′-GGAGGGAGAAAACTCCTTGGA-3′
Reverse: 5′-GGCCAGTAGGTTGCACATTGT-3′
Human IFIT1: forward: 5′-TCAGGTCAAGGATAGTCTGGAG-3′
Reverse: 5′-AGGTTGTGTATTCCCACACTGTA-3′
Human NLRP3: forward: 5′-GATCTTCGCTGCGATCAACAG-3′
Reverse: 5′-CGTGCATTATCTGAACCCCAC-3′
Human RPL13A: forward: 5′-GCCATCGTGGCTAAACAGGTA-3′
Reverse: 5′-GTTGGTGTTCATCCGCTTGC-3′
Mouse IFN-β: forward: 5′-CAGCTCCAAGAAAGGACGAAC-3′
Reverse: 5′-GGCAGTGTAACTCTTCTGCAT-3′
Mouse GAPDH: forward: 5′-GAAGGGCTCATGACCACAGT-3′
Reverse: 5′-GGATGCAGGGATGATGTTCT-3′
ZIKV genomic RNA: forward: 5′-TTGGTCATGATACTGCTGATTG C-3′
Reverse: 5′-CCYTCCACRAAGTCYCTATTGC-3′

Knockdown of NLRP3 by RNA interference

NLRP3 siRNA and control (scramble) siRNA were obtained from Transheep and transfected into PBMCs with RNAiMAX (Invitrogen), according to manufacturer's instruction. RNA oligonucleotides used in this study are as follows:

NLRP3 siRNA#1 forward: GGAAGUGGACUGCGAGAAGUU
Reverse: AACUUCUCGCAGUCCACUUCC
NLRP3 siRNA#2 forward: GCUGUAACAUUCGGAGAUUGU
Reverse: ACAAUCUCCGAAUGUUACAGC

Viral plaque titration

The ZIKV-containing supernatants were collected. Vero cells were infected with ZIKV supernatants for 1 h at room temperature as described (Wu *et al*, 2017). After washing with PBS, the plate was overlaid with Dulbecco's modified Eagle's medium containing 1% low melting-point agarose and incubate at 37°C for 72 h before crystal violet staining.

Measurement of cytokines

Human IL-1β in cell culture supernatants was detected with an ELISA kit (BD Biosciences, No. 557953) according to the manufacturer's protocols. Human IL-18 in cell supernatants was detected with an ELISA kit (MBL, 7620) according to the manufacturer's protocols. Human IFN-β in cell supernatants was detected with an ELISA kit (Cloud-Clone Corp, SEA222Hu) according to the manufacturer's protocols. Mouse IL-1β in cell culture supernatants was detected with an ELISA kit (BD Biosciences, No. 559603) according to the manufacturer's protocols. Mouse IFN-β in brains was detected with an ELISA kit (Cloud-Clone Corp, SEA222Mu) according to the manufacturer's protocols.

Caspase-1-mediated inflammasome activation assay

THP-1 cells or 293T cells were seeded in 12-well plates overnight before changed to Opti-MEM, and then, the cells were primed with LPS (500 ng/ml) for 3 h followed by various inflammasome ligands stimulation. For NLRP3 inflammasome activation, the cells were treated with ATP (5 mM) or poly (I:C) (2 mg/ml) for 6 h. Culture supernatants of THP-1 or 293T cells treated with indicated stimuli were precipitated by adding an equal volume of methanol and 0.25 volumes of chloroform. The supernatant mixtures were vortexed and then centrifuged for 15 min at 16,000 *g*. The upper phase was discard, and 500 μl methanol was added to the interphase. This mixture was centrifuged for 15 min at 16,000 *g* and the protein pellet was dried at 55°C, followed by immunoblot analysis to detect mature IL-1β (p17) and mature caspase-1 (p20) fragment, respectively.

Cytotoxicity assay

Relevant cells were treated as indicated. Cell death was measured by a lactate dehydrogenase (LDH) assay using CytoTox 96 Non-Radioactive Cytotoxicity Assay kit (Promega).

Quantification of cGAS-bound DNA

Flag-cGAS THP-1 cells were infected with either MOCK or ZIKV (MOI = 5) for 36 h, and then, the cell extracts were immunoprecipitated by anti-Flag beads. Immunoprecipitates were washed with low-salt lysis buffer and eluted with TE buffer then incubate at 65°C overnight. Finally, DNA precipitation was carried out with isopropanol and analyzed by qRT–PCR. Under each of the conditions (Mock or ZIKV), 20 ng of a purified plasmid encoding for the EGFP gene was added. The mix of endogenous DNA and EGFP plasmid was used to quantify the presence of specific DNA fragments. Primer sets for human mtDNA are previously described (Aguirre *et al*, 2017), and the sequences are shown below. Relative levels of the DNA molecules of interest were calculated based on the Ct values of EGFP gene amplification using the following primers: EGFP-F: ACGGCGACGTAAACGGCCAC, EGFP-R: GCACGCCGTAGG CTAGGGTG; hMyc-F: AAGGACTATCCTGCTGCCAA, hMyc-R: CCT CTTGACATTCTCCTCGG; 18S-F: TAGAGGGACAAGTGGCGTTC, 18S-R: CGCTGAGCCAGTCAGTGT; mtDNA1-F: CACCCAAGAACAGGGTT TGT, mtDNA1-R:TGGCCATGGGTATGTTGTTAA; mtDNA2-F: CTAT CACCCTATTAACCACTCA, mtDNA2-R:TTCGCCTGTAATATTGAA CGTA; mtDNA3-F:AATCGAGTAGTACTCCCGATTG, mtDNA3-R: TTCTAGGACGATGGGCATGAAA; mtDNA4-F: AATCCAAGCCTAC GTTTTCACA, mtDNA4-R: AGTATGAGGAGCGTTATGGAGT.

Statistical analysis

The results of all quantitative experiments are reported as mean ± SEM of three independent experiments, and Student's *t*-test or one-way ANOVA with Tukey's post hoc test was used for statistical analyses with the GraphPad Prism 5.0 software.

References

Aguirre S, Luthra P, Sanchez-Aparicio MT, Maestre AM, Patel J, Lamothe F, Fredericks AC, Tripathi S, Zhu T, Pintado-Silva J, Webb LG, Bernal-Rubio D, Solovyov A, Greenbaum B, Simon V, Basler CF, Mulder LC, Garcia-Sastre A, Fernandez-Sesma A (2017) Dengue virus NS2B protein targets cGAS for degradation and prevents mitochondrial DNA sensing during infection. *Nat Microbiol* 2: 17037

Akira S, Uematsu S, Takeuchi O (2006) Pathogen recognition and innate immunity. *Cell* 124: 783–801

Barral PM, Sarkar D, Fisher PB, Racaniello VR (2009) RIG-I is cleaved during picornavirus infection. *Virology* 391: 171–176

Bowen JR, Zimmerman MG, Suthar MS (2018) Taking the defensive: immune control of Zika virus infection. *Virus Res* 254: 21–26

Chan YK, Gack MU (2016) Viral evasion of intracellular DNA and RNA sensing. *Nat Rev Microbiol* 14: 360–373

Chen M, Meng Q, Qin Y, Liang P, Tan P, He L, Zhou Y, Chen Y, Huang J, Wang RF, Cui J (2016) TRIM14 inhibits cGAS degradation mediated by selective autophagy receptor p62 to promote innate immune responses. *Mol Cell* 64: 105–119

Cheong WC, Kang HR, Yoon H, Kang SJ, Ting JP, Song MJ (2015) Influenza A virus NS1 protein inhibits the NLRP3 inflammasome. *PLoS ONE* 10: e0126456

Dick GW, Kitchen SF, Haddow AJ (1952) Zika virus. I. Isolations and serological specificity. *Trans R Soc Trop Med Hyg* 46: 509–520

Dinarello CA (2009) Immunological and inflammatory functions of the interleukin-1 family. *Annu Rev Immunol* 27: 519–550

Fernandez-Garcia MD, Mazzon M, Jacobs M, Amara A (2009) Pathogenesis of flavivirus infections: using and abusing the host cell. *Cell Host Microbe* 5: 318–328

Gack MU, Albrecht RA, Urano T, Inn KS, Huang IC, Carnero E, Farzan M, Inoue S, Jung JU, Garcia-Sastre A (2009) Influenza A virus NS1 targets the ubiquitin ligase TRIM25 to evade recognition by the host viral RNA sensor RIG-I. *Cell Host Microbe* 5: 439–449

Grant A, Ponia SS, Tripathi S, Balasubramaniam V, Miorin L, Sourisseau M, Schwarz MC, Sanchez-Seco MP, Evans MJ, Best SM, Garcia-Sastre A (2016) Zika virus targets human STAT2 to inhibit type I interferon signaling. *Cell Host Microbe* 19: 882–890

Hasdemir B, Murphy JE, Cottrell GS, Bunnett NW (2009) Endosomal deubiquitinating enzymes control ubiquitination and down-regulation of protease-activated receptor 2. *J Biol Chem* 284: 28453–28466

Hilgenfeld R (2016) Zika virus NS1, a pathogenicity factor with many faces. *EMBO J* 35: 2631–2633

Ioos S, Mallet HP, Leparc Goffart I, Gauthier V, Cardoso T, Herida M (2014) Current Zika virus epidemiology and recent epidemics. *Med Mal Infect* 44: 302–307

Jabir MS, Ritchie ND, Li D, Bayes HK, Tourlomousis P, Puleston D, Lupton A, Hopkins L, Simon AK, Bryant C, Evans TJ (2014) Caspase-1 cleavage of the TLR adaptor TRIF inhibits autophagy and beta-interferon production during Pseudomonas aeruginosa infection. *Cell Host Microbe* 15: 214–227

Khaiboullina SF, Uppal T, Sarkar R, Gorzalski A, St Jeor S, Verma SC (2017) ZIKV infection regulates inflammasomes pathway for replication in monocytes. *Sci Rep* 7: 16050

Komune N, Ichinohe T, Ito M, Yanagi Y (2011) Measles virus V protein inhibits NLRP3 inflammasome-mediated interleukin-1beta secretion. *J Virol* 85: 13019–13026

Kumar A, Hou S, Airo AM, Limonta D, Mancinelli V, Branton W, Power C, Hobman TC (2016) Zika virus inhibits type-I interferon production and downstream signaling. *EMBO Rep* 17: 1766–1775

Labbe K, McIntire CR, Doiron K, Leblanc PM, Saleh M (2011) Cellular inhibitors of apoptosis proteins cIAP1 and cIAP2 are required for efficient caspase-1 activation by the inflammasome. *Immunity* 35: 897–907

Lee H, Shin EA, Lee JH, Ahn D, Kim CG, Kim JH, Kim SH (2018) Caspase inhibitors: a review of recently patented compounds (2013-2015). *Expert Opin Ther Pat* 28: 47–59

Li C, Xu D, Ye Q, Hong S, Jiang Y, Liu X, Zhang N, Shi L, Qin CF, Xu Z (2016) Zika virus disrupts neural progenitor development and leads to microcephaly in mice. *Cell Stem Cell* 19: 672

Liu T, Tang Q, Liu K, Xie W, Liu X, Wang H, Wang RF, Cui J (2016) TRIM11 suppresses AIM2 inflammasome by degrading AIM2 via p62-dependent selective autophagy. *Cell Rep* 16: 1988–2002

Manangeeswaran M, Ireland DD, Verthelyi D (2016) Zika (PRVABC59) infection is associated with T cell infiltration and neurodegeneration in CNS of immunocompetent neonatal C57Bl/6 mice. *PLoS Pathog* 12: e1006004

Martinon F, Mayor A, Tschopp J (2009) The inflammasomes: guardians of the body. *Annu Rev Immunol* 27: 229–265

Miner JJ, Cao B, Govero J, Smith AM, Fernandez E, Cabrera OH, Garber C, Noll M, Klein RS, Noguchi KK, Mysorekar IU, Diamond MS (2016) Zika virus infection during pregnancy in mice causes placental damage and fetal demise. *Cell* 165: 1081–1091

Miner JJ, Diamond MS (2017) Zika virus pathogenesis and tissue tropism. *Cell Host Microbe* 21: 134–142

Nijman SM, Luna-Vargas MP, Velds A, Brummelkamp TR, Dirac AM, Sixma TK, Bernards R (2005) A genomic and functional inventory of deubiquitinating enzymes. *Cell* 123: 773–786

Parekh FK, Davison BB, Gamboa D, Hernandez J, Branch OH (2010) Placental histopathologic changes associated with subclinical malaria infection and its impact on the fetal environment. *Am J Trop Med Hyg* 83: 973–980

Park EK, Jung HS, Yang HI, Yoo MC, Kim C, Kim KS (2007) Optimized THP-1 differentiation is required for the detection of responses to weak stimuli. *Inflamm Res* 56: 45–50

Petersen E, Wilson ME, Touch S, McCloskey B, Mwaba P, Bates M, Dar O, Mattes F, Kidd M, Ippolito G, Azhar EI, Zumla A (2016) Rapid spread of zika virus in the Americas-implications for public health preparedness for mass gatherings at the 2016 Brazil Olympic games. *Int J Infect Dis* 44: 11–15

Pierson TC, Diamond MS (2013) Flaviviruses. In *Fields virology*, Knipe DM, Howley PM (eds), 6th edn, pp 747–794. Philadelphia, PA: Wolters Kluwer/Lippincott Williams & Wilkins

Pu SY, Wu RH, Yang CC, Jao TM, Tsai MH, Wang JC, Lin HM, Chao YS, Yueh A (2011) Successful propagation of flavivirus infectious cDNAs by a novel method to reduce the cryptic bacterial promoter activity of virus genomes. *J Virol* 85: 2927–2941

Radivojac P, Vacic V, Haynes C, Cocklin RR, Mohan A, Heyen JW, Goebl MG, Iakoucheva LM (2010) Identification, analysis, and prediction of protein ubiquitination sites. *Proteins* 78: 365–380

Rossi SL, Tesh RB, Azar SR, Muruato AE, Hanley KA, Auguste AJ, Langsjoen RM, Paessler S, Vasilakis N, Weaver SC (2016) Characterization of a novel murine model to study Zika virus. *Am J Trop Med Hyg* 94: 1362–1369

Rubin EJ, Greene MF, Baden LR (2016) Zika virus and microcephaly. *N Engl J Med* 374: 984–985

Schneider WM, Chevillotte MD, Rice CM (2014) Interferon-stimulated genes: a complex web of host defenses. *Annu Rev Immunol* 32: 513–545

Schoggins JW, MacDuff DA, Imanaka N, Gainey MD, Shrestha B, Eitson JL, Mar KB, Richardson RB, Ratushny AV, Litvak V, Dabelic R, Manicassamy B, Aitchison JD, Aderem A, Elliott RM, Garcia-Sastre A, Racaniello V, Snijder EJ, Yokoyama WM, Diamond MS *et al* (2014) Pan-viral specificity of IFN-induced genes reveals new roles for cGAS in innate immunity. *Nature* 505: 691–695

Schwarz MC, Sourisseau M, Espino MM, Gray ES, Chambers MT, Tortorella D, Evans MJ (2016) Rescue of the 1947 Zika virus prototype strain with a cytomegalovirus promoter-driven cDNA clone. *mSphere* 1: e00246-16

Shan C, Muruato AE, Jagger BW, Richner J, Nunes BTD, Medeiros DBA, Xie X, Nunes JGC, Morabito KM, Kong WP, Pierson TC, Barrett AD, Weaver SC, Rossi SL, Vasconcelos PFC, Graham BS, Diamond MS, Shi PY (2017) A single-dose live-attenuated vaccine prevents Zika virus pregnancy transmission and testis damage. *Nat Commun* 8: 676

Shrivastava G, Leon-Juarez M, Garcia-Cordero J, Meza-Sanchez DE, Cedillo-Barron L (2016) Inflammasomes and its importance in viral infections. *Immunol Res* 64: 1101–1117

Taxman DJ, Huang MT, Ting JP (2010) Inflammasome inhibition as a pathogenic stealth mechanism. *Cell Host Microbe* 8: 7–11

Tricarico PM, Caracciolo I, Crovella S, D'Agaro P (2017) Zika virus induces inflammasome activation in the glial cell line U87-MG. *Biochem Biophys Res Comm* 492: 597–602

Wang Q, Liu X, Cui Y, Tang Y, Chen W, Li S, Yu H, Pan Y, Wang C (2014) The E3 ubiquitin ligase AMFR and INSIG1 bridge the activation of TBK1 kinase by modifying the adaptor STING. *Immunity* 41: 919–933

Wang Y, Ning X, Gao P, Wu S, Sha M, Lv M, Zhou X, Gao J, Fang R, Meng G, Su X, Jiang Z (2017) Inflammasome activation triggers caspase-1-mediated cleavage of cGAS to regulate responses to DNA virus infection. *Immunity* 46: 393–404

Wang W, Li G, De W, Luo Z, Pan P, Tian M, Wang Y, Xiao F, Li A, Wu K, Liu X, Rao L, Liu F, Liu Y, Wu J (2018) Zika virus infection induces host inflammatory responses by facilitating NLRP3 inflammasome assembly and interleukin-1beta secretion. *Nat Commun* 9: 106

Winkler S, Rosen-Wolff A (2015) Caspase-1: an integral regulator of innate immunity. *Semin Immunopathol* 37: 419–427

Wu Y, Liu Q, Zhou J, Xie W, Chen C, Wang Z, Yang H, Cui J (2017) Zika virus evades interferon-mediated antiviral response through the co-operation of multiple nonstructural proteins *in vitro*. *Cell Discov* 3: 17006

Xia H, Luo H, Shan C, Muruato AE, Nunes BTD, Medeiros DBA, Zou J, Xie X, Giraldo MI, Vasconcelos PFC, Weaver SC, Wang T, Rajsbaum R, Shi PY (2018) An evolutionary NS1 mutation enhances Zika virus evasion of host interferon induction. *Nat Commun* 9: 414